NASA CONTRACTOR REPORT

NASA CR-2588

NASA CR-2

2. u/u

4.

VIBRATION OF SKEWED CANTILEVER PLATES AND HELICOIDAL SHELLS

D. P. Beres and C. D. Bailey

5.

NATIONAL AERONAUTICS AND SPACE ADMINISTRATION • WASHINGTON, D. C. • SEPTEMBER 1975

1. Report No. NASA CR-2588	2. Government Accession No.	3. Recipient's Catalog No.
4. Title and Subtitle VIBRATION OF SKEWED CANTILEVER PLATES AND HELICOIDAL SHELLS		5. Report Date September 1975
		6. Performing Organization Code
7. Author(s) D. P. BERES and C. D. BAILEY		8. Performing Organization Report No.
		10. Work Unit No.
9. Performing Organization Name and Address The Ohio State University Aero-Astro Engineering Dept. Columbus, Ohio 43210		11. Contract or Grant No. NGR 36-008-197
		13. Type of Report and Period Covered Contractor Report
12. Sponsoring Agency Name and Address National Aeronautics and Space Administration Washington, D. C. 20546		14. Sponsoring Agency Code

15. Supplementary Notes

Topical report.

16. Abstract

Theoretical vibration frequencies and mode shapes are obtained for skewed plates and helicoidal shells with a cantilever boundary. Using Hamilton's Law of Varying Action, a power series solution is developed to obtain converged numerical results for the five lowest frequencies. Effects of geometrical variables such as aspect ratio, sweep angle and shell radius-to-thickness ratio are investigated. Accuracy of solution method is substantiated by comparison with existing skewed plate spherical caps, and conical shell results.

17. Key Words (Suggested by Author(s)) Vibration, plates, shells, skewed, helicoidal	18. Distribution Statement Unclassified - Unlimited Subject Category 39 Structural Mechanics		
19. Security Classif. (of this report) Unclassified	20. Security Classif. (of this page) Unclassified	21. No. of Pages 80	22. Price* $4.75

SUMMARY

The vibration eigenvalues and modes have been analytically determined for the helicoidal shell and its limiting case, the skewed flat plate. A general analysis is given wherein the energy equation employed is derived from Hamilton's Law of Varying Action. No numerical data has been found in the literature for the helicoidal shell. Results for spherical caps and complete conical shells, obtained by the method of this paper, are compared to exact solutions from the literature for these two shell geometries. The authors consider this paper to be a significant step toward an analytical solution to the thermally stressed, variable thickness, turbine blade immersed in both a fluid flow field and in an acceleration field.

TABLE OF CONTENTS

LIST OF TABLES

LIST OF ILLUSTRATIONS

LIST OF SYMBOLS

A,B	Lame geometric parameters
A_{ij}, B_{ij}, C_{ij}	Unknown coefficients in the assumed solution
b	Half-width of the skewed plate
C	Membrane stiffness parameter
D	Bending stiffness parameter
d	Ordinary differential operator
E	Young's modulus
e	Exponential function
e_x, e_y, e_{xy}	Total strains in the body, principal and shearing; independent of time
$\bar{e}_x, \bar{e}_y, \bar{e}_{xy}$	Total strains in the body, principal and shearing; time dependent
$F_{B_x}, F_{B_y}, F_{B_z}$	Body forces in the x,y,z directions respectively
$F_{S_x}, F_{S_y}, F_{S_z}$	Surface forces in the x,y,z directions respectively
h	Shell or plate thickness
i,j,k,ℓ	Subscripts and supercripts denoting indicies
K_x, K_y, K_{xy}	Bending strains, principal and shearing
ℓ	Slant length of the skewed plate and helicoidal shell
ℓ^*	Slant length for conical shell
M,N	Integers
N^*	Stiffness parameter for conical shell
q_i	The i th generalized coordinate
R	Radius of the cylinder and helicoidal shell

R_x, R_y	Principal radii of curvature in the x and y directions
T	Kinetic energy
t	Independent variable time
t_0	Time when observation of the system begins
t_1	Time when observation of the system ends
u, v, w	Displacements of the body in the x,y,z directions respectively; independent of time
$\bar{u}, \bar{v}, \bar{w}$	Displacements of the body in the x,y,z directions respectively; time dependent
W	Work
x, y	Orthogonal curvilinear surface coordinates; as subscripts they denote partial differentiation, except as otherwise noted in this list of symbols
x_0, x_1	Extremeties of the structure in the x direction; constants
y_0, y_1	Extremeties of the structure in the y direction; functions of x
z	Coordinate normal to the middle surface
α	Skew angle
β	Half-angle for the conical shell
γ	Half-angle for the helicoidal shell
δ	Variational operator
$\varepsilon_x, \varepsilon_y, \varepsilon_{xy}$	Membrane strains, principal and shearing
η, ξ	Non-dimensional skewed coordinates; as subscripts they denote partial differentiation
$\bar{\eta}, \bar{\xi}$	Dimensional skewed coordinates

LIST OF SYMBOLS (continued)

λ^*	Frequency parameter for spherical and conical shells
λ_p	Frequency parameter for the skewed plate
λ_s	Frequency parameter for the helicoidal shell
ν	Poisson's ratio
ρ	Mass density
Σ	Denotes summation
$\sigma_x, \sigma_y, \sigma_{xy}$	Total stresses in the body, principal and shearing; independent of time
$\bar{\sigma}_x, \bar{\sigma}_y, \bar{\sigma}_{xy}$	Total stresses in the body, principal and shearing; time dependent
σ_z	Stress normal to the middle surface
ϕ	Opening angle for the spherical shell
ω	Natural radial frequency of a vibrating system
∂	Partial differential operator
$\cdot$	Superscript denoting differentiation with respect to time

INTRODUCTION

In recent years emphasis in solid mechanics has shifted
from plates to shells. This can be attributed to the fact
that thin plate vibrations have been widely explored for
simple geometries such as the circle, the rectangle, and the
rhombus [1]. Exact solutions were found for isolated cases.
However, for many boundary conditions the analyst was (and
is) forced to seek an approximate solution. "Approximate"
usually meant a Rayleigh-Ritz type solution. "Beam" func-
tions became popular among plate analysts who attempted
solutions by Rayleigh-Ritz since they already satisfied the
geometric boundary conditions. The results in many cases
were less than satisfactory. This inaccuracy was generally
attributed to the fact that the method was "approximate".

With the advent of finite element analysis, the analyst
had at his disposal an approximate method which took much
less intuition than Rayleigh-Ritz (the Rayleigh-Ritz method
requires one to assume a solution in the form of "admissible
functions). A predominance of the finite element technique
has come about for numerous reasons, but two major factors
are the easy satisfaction of the boundary conditions and the
ease of handling complicated geometric shapes. However, us-
ing concepts long understood for satisfaction of boundary
conditions [2], the Ritz method can now be applied to geo-
metrically complicated structures with great accuracy for
both stationary and non-stationary problems.

Since finite element analysis is now widely accepted as
the best way to solve the difficult problems, the Rayleigh-
Ritz procedure has been pushed aside [3]. In the authors'
opinion, it is unfortunate that analysts always think of
Rayleigh-Ritz instead of just Ritz [4]. Rayleigh's intent
was that of choosing one function, which if at all close to
the true mode shape, would yield a fair, if not good,
approximation for the frequency by means of Rayleigh's quo-
tient. However, Ritz's idea was that of choosing a series
of suitable approximating functions. Ritz [4] showed that
such a series, with a finite number of terms, converges to
an upper bound of the true solution. His proof, however, and
the resulting direct solutions apply only to stationary
systems. Using concepts [5] associated with Hamilton's Law
of Varying Action [6] the authors have obtained direct solu-
tions to non-stationary and/or non-conservative systems.
When calculating the transient motion of a deformable body,
a major simplification for achieving direct solutions (as
with the equations of Lagrange) results when one uses the
free vibration modes and normal coordinates, whether or not
this procedure uncouples the system. Thus, the generation
of free vibration modes and frequencies continues to be of
great importance in the solution of the problems of the

displacement or motion of physical systems. As a result, the authors have restricted this paper to a particularly difficult (and unsolved to the author's knowledge) but conservative, stationary problem: the free vibration modes and frequencies of a helicoidal shell.

A fact which seems to have been overlooked, possibly because of the concepts associated with the Rayleigh-Ritz method, is the accuracy obtainable when power series are taken as the "admissible" functions. In this paper, Appendix I, and in other work, the degree of accuracy which can be obtained by direct solutions of the energy equation has been compared by the authors to exact solutions where available. In all applications (particles, rigid bodies, beams, plates, and shells), when finite time intervals and finite space intervals are properly employed, the degree of accuracy far surpassed expectations. The Ritz method, in every case, converged to the exact solution, for the constraints assumed, in the same sense that any number representing the solution to a transcendental equation can be considered to be exact. The results of these endeavors all indicate that the idea of "approximation" associated with the Rayleigh concept should not be associated with the Ritz method.

As mentioned above, this study is restricted to the stationary problem of simple harmonic vibrations. For the helicoidal shell, the displacement field is completely described by the displacements u, v, and w, all three of which are functions of the orthogonal surface coordinates x and y. In the limiting case of the flat plate, only w is considered, where w is a function of the rectangular inplane coordinates x and y. Inplane (or membrane) vibration for the flat plate will not be treated, although the authors have completed such solutions for the rectangular cantilever plate [2]. As has been shown for a completely free elliptical plate [7], and for plates with various other boundary conditions (Refs. [2], [8], when power series are used the Ritz method yields very accurate mode shapes as well as accurate frequencies.

2

CHAPTER I.

THEORY

Hamilton's Law

In attempting an energy solution, it seems that the
analyst is always confronted with which energy equation or
theorem to use as a starting point. One form which embodies
all other energy equations of the mechanics of solids, is
that enunciated in 1834 by Sir William Rowan Hamilton [6]
and called by him the "Law of Varying Action". It is not
the well known Hamilton's Principle. Indeed Hamilton's
Principle is a special case of Hamilton's Law (throughout
the text Hamilton's Law will refer to the Law of Varying
Action). Hamilton's Principle is usually written [9] as,

$$\delta \int_{t_0}^{t_1} (T + W) \, dt = 0 \tag{1}$$

where T is the total kinetic energy of the system and W is
the total work of forces acting on or within the system.
Hamilton's Law, which is much more general [6], is expressed
as,

$$\delta \int_{t_0}^{t_1} (T + W) \, dt - \frac{\partial T}{\partial \dot{q}_i} \, \delta q_i \, \Big|_{t_0}^{t_1} = 0 \tag{2}$$

In the variational calculus, a stationary solution is, by
definition, a solution of a given system for which

$$\frac{\partial T}{\partial \dot{q}_i} \, \delta q_i \, \Big|_{t_0}^{t_1} = 0.$$ Eq. (2), which reduces to Eq. (1) for

stationary motion, applies to non-stationary motion as well
[5]. No matter what the motion is, Eq. (2) will yield either
a direct solution (as in this paper) or the differential
equations of the system.

Strain-Displacement Equations

It is assumed that the material of the shell is isotropic
and obeys a linear stress-strain relationship. In addition,
it is assumed that the oscillations cause infinitesimal dis-
placements which can be described by a set of linear strain-
displacement relations. These strain-displacement relations
come about as a result of considering the deformation of the

3

middle surface.   The additional assumption that normals to the middle surface remain normal throughout the deformation process, always made in thin shell theory, then locates all other points in the body relative to the middle surface. Since differential geometry is not the topic of this paper the authors will merely restate the linear strain-displacement relations for thin shells given by Novozhilov [10].

$$\varepsilon_x = \frac{1}{A}\frac{\partial \overline{u}}{\partial x} + \frac{1}{AB}\frac{\partial A}{\partial y}\overline{v} + \frac{1}{R_x}\overline{w}$$

$$\varepsilon_y = \frac{1}{B}\frac{\partial \overline{v}}{\partial y} + \frac{1}{AB}\frac{\partial B}{\partial x}\overline{u} + \frac{1}{R_y}\overline{w}$$

$$\varepsilon_{xy} = \frac{B}{A}\frac{\partial}{\partial x}(\overline{v}/B) + \frac{A}{B}\frac{\partial}{\partial y}(\overline{u}/A)$$

$$K_x = \frac{-1}{A}\frac{\partial}{\partial x}\left(\frac{1}{A}\frac{\partial \overline{w}}{\partial x} - \frac{\overline{u}}{R_x}\right) - \frac{1}{AB}\frac{\partial A}{\partial y}\left(\frac{1}{B}\frac{\partial \overline{w}}{\partial y} - \frac{\overline{v}}{R_y}\right)$$

$$K_y = -\frac{1}{B}\frac{\partial}{\partial y}\left(\frac{1}{B}\frac{\partial \overline{w}}{\partial y} - \frac{\overline{v}}{R_y}\right) - \frac{1}{AB}\frac{\partial B}{\partial x}\left(\frac{1}{A}\frac{\partial \overline{w}}{\partial x} - \frac{\overline{u}}{R_x}\right)$$

$$K_{xy} = -\frac{2}{AB}\left(\frac{\partial^2 \overline{w}}{\partial x \partial y} - \frac{1}{A}\frac{\partial A}{\partial y}\frac{\partial \overline{w}}{\partial x} - \frac{1}{B}\frac{\partial B}{\partial x}\frac{\partial \overline{w}}{\partial y}\right)$$

$$+ \frac{2}{R_x}\left(\frac{1}{B}\frac{\partial \overline{u}}{\partial y} - \frac{1}{AB}\frac{\partial A}{\partial y}\overline{u}\right) + \frac{2}{R_y}\left(\frac{1}{A}\frac{\partial \overline{v}}{\partial x} - \frac{1}{AB}\frac{\partial B}{\partial x}\overline{v}\right) \qquad (3)$$

For any point on the surface of a right circular cylinder, where x is the axis of the cylinder and y is the circumferential angle measured from the vertical (clockwise positive, see Fig. 3), the following geometrical relations are true:

$$R_x = \infty$$

$$R_y = R = \text{constant}$$

$$A = 1$$

$$B = R = \text{constant}$$

4

$$\frac{\partial A}{\partial y} = \frac{\partial A}{\partial x} = \frac{\partial B}{\partial y} = \frac{\partial B}{\partial x} = \frac{\partial}{\partial y}(R_x) = \frac{\partial}{\partial x}(R_x) = \frac{\partial}{\partial y}(R_y) = \frac{\partial}{\partial x}(R_y) = 0 \quad (4)$$

where R is the radius of the cylinder. With these simplifications Eq. (3) becomes,

$$\epsilon_x = \frac{\partial \bar{u}}{\partial x}$$

$$\epsilon_y = \frac{1}{R}\left(\frac{\partial \bar{v}}{\partial y} + \bar{w}\right)$$

$$\epsilon_{xy} = \frac{\partial \bar{v}}{\partial x} + \frac{1}{R}\frac{\partial \bar{u}}{\partial y}$$

$$K_x = -\frac{\partial^2 \bar{w}}{\partial x^2}$$

$$K_y = -\frac{1}{R^2}\frac{\partial^2 \bar{w}}{\partial y^2} + \frac{1}{R^2}\frac{\partial \bar{v}}{\partial y}$$

$$K_{xy} = -\frac{2}{R}\frac{\partial^2 \bar{w}}{\partial x \partial y} + \frac{2}{R}\frac{\partial \bar{v}}{\partial x} \quad (5)$$

The total strain of any point in the body is given by,

$$\bar{e}_x = \epsilon_x + z\,K_x$$

$$\bar{e}_y = \epsilon_y + z\,K_y$$

$$\bar{e}_{xy} = \epsilon_{xy} + z\,K_{xy} \quad (6)$$

where z is the distance from the middle surface. For the plane stress problem (that is σ_z is negligible, thin shell assumption) the stress at any point in the body is given by,

$$\bar{\sigma}_x = \frac{E}{(1-\nu^2)}(\bar{e}_x + \nu\,\bar{e}_y)$$

$$\bar{\sigma}_y = \frac{E}{(1-\nu^2)}(\bar{e}_y + \nu\,\bar{e}_x)$$

$$\bar{\sigma}_{xy} = \frac{E}{2(1+\nu)}\,\bar{e}_{xy} \quad (7)$$

5

Work

For an elastic body, the work, W, is that due to the internal elastic restoring forces, the internal or "body" forces, and the external or surface forces:

$$W = - \iiint (\bar{\sigma}_x \, \bar{e}_x + \bar{\sigma}_y \, \bar{e}_y + \bar{\sigma}_{xy} \, \bar{e}_{xy}) \, R \, dx \, dy \, dz$$

$$+ \iiint (F_{B_x} \, \bar{u} + F_{B_y} \, \bar{v} + F_{B_z} \, \bar{w}) \, R \, dx \, dy \, dz$$

$$+ \iint (F_{S_x} \, \bar{u} + F_{S_y} \, \bar{v} + F_{S_z} \, \bar{w}) \, dS \qquad (8)$$

Taking the variation of Eq. (8) with respect to the displacements (as in the principle of virtual work) yields,

$$\delta W = - \iiint (\bar{\sigma}_x \, \delta \bar{e}_x + \bar{\sigma}y \, \delta \bar{e}_y + \bar{\sigma}_{xy} \, \delta \bar{e}_{xy}) \, R \, dx \, dy \, dz$$

$$+ \iiint (F_{B_x} \, \delta \bar{u} + F_{B_y} \, \delta \bar{v} + F_{B_z} \, \delta \bar{w}) \, R \, dx \, dy \, dz$$

$$+ \iint (F_{S_x} \, \delta \bar{u} + F_{S_y} \, \delta \bar{v} + F_{S_z} \, \delta \bar{w}) \, dS \qquad (9)$$

Kinetic Energy

Rotary inertia is negligible for thin plate and thin shell vibrations, thus, neglecting rotary inertia, the total kinetic energy is,

$$T = \frac{1}{2} \iiint \rho \, (\dot{\bar{u}}^2 + \dot{\bar{v}}^2 + \dot{\bar{w}}^2) \, R \, dx \, dy \, dz \qquad (10)$$

and

$$\frac{\partial T}{\partial \dot{q}_i} \, \delta q_i \, \Big|_{t_0}^{t_1} = \iiint \rho (\dot{\bar{u}} \, \delta \bar{u} + \dot{\bar{v}} \, \delta \bar{v} + \dot{\bar{w}} \, \delta \bar{w}) \, R \, dxdydz \, \Big|_{t_0}^{t_1} \qquad (11)$$

Taking the variation of Eq. (10) and substracting Eq. (11) in Hamilton's Law,

6

$$\int_{t_0}^{t_1} \delta T \ dt \ - \ \frac{\partial T}{\partial \dot{q}_1} \ \delta q_i \ \Big|_{t_0}^{t_1} \ =$$

$$\int_{t_0}^{t_1} \Big[\ \iiint \rho (\dot{\overline{u}} \ \delta \dot{\overline{u}} + \dot{\overline{v}} \ \delta \dot{\overline{v}} + \dot{\overline{w}} \ \delta \dot{\overline{w}}) \ R \ dx \ dy \ dz \ \Big] \ dt$$

$$- \iiint \rho (\dot{\overline{u}} \ \delta \overline{u} + \dot{\overline{v}} \ \delta \overline{v} + \dot{\overline{w}} \ \delta \overline{w}) R \ dx \ dy \ dz \ \Big|_{t_0}^{t_1} \qquad (12)$$

Integrating the first term on the right hand side of Eq. (12) by parts with respect to time yields,

$$\int_{t_0}^{t_1} \delta T \ dt \ - \ \frac{\partial T}{\partial \dot{q}_i} \ \delta q_i \ \Big|_{t_0}^{t_1} \ =$$

$$- \int_{t_0}^{t_1} \Big[\iiint \rho (\ddot{\overline{u}} \ \delta \overline{u} + \ddot{\overline{v}} \ \delta \overline{v} + \ddot{\overline{w}} \ \delta \overline{w}) R \ dx \ dy \ dz \Big] \cdot \ dt \qquad (13)$$

Energy Equation

Substituting Eqs. (9) and (13) into Eq. (12), the energy equation (Hamilton's Law) becomes,

$$\int_{t_0}^{t_1} \Big[-\iiint \rho (\ddot{\overline{u}} \ \delta \overline{u} + \ddot{\overline{v}} \ \delta \overline{v} + \ddot{\overline{w}} \ \delta \overline{w}) R \ dx \ dy \ dz$$

$$-\iiint (\overline{\sigma}_x \ \delta \overline{e}_x + \overline{\sigma}_y \ \delta \overline{e}_y + \overline{\sigma}_{xy} \ \delta \overline{e}_{xy}) R \ dx \ dy \ dz$$

$$+\iiint (F_{B_x} \ \delta \overline{u} + F_{B_y} \ \delta \overline{v} + F_{B_z} \ \delta \overline{w}) R \ dx \ dy \ dz$$

$$+\iint (F_{S_x} \ \delta \overline{u} + F_{S_y} \ \delta \overline{v} + F_{S_z} \ \delta \overline{w}) dS \ \Big] \ dt = 0 \qquad (14)$$

7

Eq. (14) applies to non-stationary as well as stationary motion. For the case of no external forces acting, assume simple harmonic motion (sin ωt or cos ωt or $e^{i\omega t}$ will all yield exactly the same result in this stationary problem)

$$\bar{u}(x,y,t) = u(x,y) \cos \omega t$$

$$\bar{v}(x,y,t) = v(x,y) \cos \omega t$$

$$\bar{w}(x,y,t) = w(x,y) \cos \omega t \qquad (15)$$

Since the strain-displacement relations are linear and the body is elastic (thus $\bar{\sigma}_x(x,y,t) = \sigma_x(x,y)\cos \omega t$, $\bar{e}_x(x,y,t) = e_x(x,y)\cos \omega t$, and likewise for $\bar{\sigma}_y$, $\bar{\sigma}_{xy}$, $\bar{e}_y$, $\bar{e}_{xy}$), Eq. (14) becomes, upon substitution of Eq. (15),

$$\left[\omega^2 \iiint \rho (u\ \delta u + v\ \delta v + w\ \delta w)R\ dx\ dy\ dz \right.$$

$$\left. - \iiint (\sigma_x\ \delta e_x + \sigma_y\ \delta e_y + \sigma_{xy}\ \delta e_{xy})R\ dx\ dy\ dz \right]$$

$$\int_{t_0}^{t_1} \cos^2 \omega t\ dt = 0 \qquad (16)$$

Since the integral on time in Eq. (16) does not vanish for any t_1 greater than t_0, one must have,

$$\omega^2 \iiint \rho (u\ \delta u + v\ \delta v + w\ \delta w)R\ dx\ dy\ dz$$

$$- \iiint (\sigma_x\ \delta e_x + \sigma_y\ \delta e_y + \sigma_{xy}\ \delta e_{xy})R\ dx\ dy\ dz = 0 \qquad (17)$$

Eq. (17) is the familiar equation of the principle of minimum potential energy which is applicable only to stationary systems. If the structure is symmetric about the middle surface, the neutral surface and middle surface are coincident. Assuming such is the case, upon substitution of Eqs. (6) and (7), Eq. (17) becomes,

8

$$\omega^2 \int_{x_0}^{x_1} \int_{y_0}^{y_1} \rho h(u \, \delta u + v \, \delta v + w \, \delta w) R \, dy \, dx$$

$$- \frac{E}{(1-\nu^2)} \int_{x_0}^{x_1} \int_{y_0}^{y_1} [h \{(\epsilon_x + \nu \, \epsilon_y) \delta \epsilon_x + (\epsilon_y + \nu \, \epsilon_x) \delta \epsilon_y$$

$$+ \frac{(1-\nu)}{2} \epsilon_{xy} \, \delta \epsilon_{xy}\} + \frac{h^3}{12} \{(K_x + \nu \, K_y) \delta K_x$$

$$+ (K_y + \nu \, K_x) \delta K_y + \frac{(1-\nu)}{2} K_{xy} \, \delta K_{xy}\} \,]R \, dy \, dx = 0 \quad (18)$$

Let $C = Eh/(1-\nu^2)$ and $D = Eh^3/12(1-\nu^2)$. Substitution of Eq. (5) into Eq. (18) yields three coupled equations in u, v, and w.

$$\int_{x_0}^{x_1} \int_{y_0}^{y_1} C \, [(u_x \, \delta u_x + \frac{(1-\nu)}{2} \, \frac{1}{R^2} \, u_y \, \delta u_y)$$

$$+ (\frac{(1-\nu)}{2} \frac{1}{R} v_x \, \delta u_y + \frac{\nu}{R} v_y \, \delta u_x) + (\frac{\nu}{R} w \, \delta u_x)]R \, dy \, dx$$

$$- \omega^2 \int_{x_0}^{x_1} \int_{y_0}^{y_1} \rho \, h(u \, \delta u) R \, dy \, dx = 0 \quad (19)$$

and,

$$\int_{x_0}^{x_1} \int_{y_0}^{y_1} [\frac{C}{R} (\frac{(1-\nu)}{2} u_y \, \delta v_x + \nu \, u_x \, \delta v_y)$$

$$+ C(\frac{1}{R^2} v_y \, \delta v_y + \frac{(1-\nu)}{2} v_x \, \delta v_x)$$

$$+ \frac{D}{R^2}(\frac{1}{R^2} v_y \, \delta v_y + 2(1-\nu)v_x \, \delta v_x)$$

$$+ \frac{C}{R^2}(w \, \delta v_y) - \frac{D}{R^2}(\frac{1}{R^2} w_{yy} \, \delta v_y + \nu \, w_{xx} \, \delta v_y$$

$$+ 2(1-\nu)w_{xy} \, \delta v_x)]R \, dy \, dx$$

$$- \omega^2 \int_{x_0}^{x_1} \int_{x_0}^{y_1} \rho h(v \, \delta v) R \, dy \, dx = 0 \quad (20)$$

9

and,

$$\int_{x_0}^{x_1} \int_{y_0}^{y_1} [\frac{C}{R}(\nu\ u_x\ \delta w) + \frac{C}{R^2}(v_y\ \delta w) - \frac{D}{R^2}(\frac{1}{R^2}\ v_y\ \delta w_{yy}$$

$$+ \nu\ v_y\ \delta w_{xx} + 2(1-\nu)v_x\ \delta w_{xy}) + \frac{C}{R^2}(w\ \delta w)$$

$$+ D\ \{w_{xx}\ \delta w_{xx} + \frac{1}{R^4}\ w_{yy}\ \delta w_{yy} + \frac{\nu}{R^2}(w_{xx}\ \delta w_{yy}$$

$$+ w_{yy}\ \delta w_{xx}) + \frac{2(1-\nu)}{R^2}\ w_{xy}\ \delta w_{xy}\}]R\ dy\ dx$$

$$- \omega^2 \int_{x_0}^{x_1} \int_{y_0}^{y_1} \rho h(w\ \delta w)R\ dy\ dx = 0 \tag{21}$$

Coordinate Transformation

If the cylinder in Fig. 3 is cut along $y = \pi$ and developed in the plane (Fig. 4), the relations between x and y and the skewed coordinates can readily be seen. They are,

$$\bar{\xi} = \frac{x}{\cos\ \alpha}$$

$$R\bar{\eta} = R\ y - x\ \tan\ \alpha \tag{22}$$

From the calculus,

$$\frac{\partial}{\partial x} = \frac{\partial}{\partial\bar{\xi}}\ \frac{\partial\bar{\xi}}{\partial x} + \frac{\partial}{\partial\bar{\eta}}\ \frac{\partial\bar{\eta}}{\partial x}$$

$$\frac{\partial}{\partial y} = \frac{\partial}{\partial\bar{\xi}}\ \frac{\partial\bar{\xi}}{\partial y} + \frac{\partial}{\partial\bar{\eta}}\ \frac{\partial\bar{\eta}}{\partial y} \tag{23}$$

Substituting Eq. (22) into Eq. (23),

10

$$\frac{\partial}{\partial x} = \frac{1}{\cos \alpha} \frac{\partial}{\partial \bar{\xi}} - \frac{\tan \alpha}{R} \frac{\partial}{\partial \bar{\eta}}$$

$$\frac{\partial}{\partial y} = \frac{\partial}{\partial \bar{\eta}}$$

$$\frac{\partial^2}{\partial y^2} = \frac{\partial^2}{\partial \bar{\eta}^2}$$

$$\frac{\partial^2}{\partial x^2} = \frac{1}{\cos^2 \alpha} \frac{\partial^2}{\partial \bar{\xi}^2} + \frac{\tan^2 \alpha}{R^2} \frac{\partial^2}{\partial \bar{\eta}^2} - \frac{2 \tan \alpha}{R \cos \alpha} \frac{\partial^2}{\partial \bar{\xi} \partial \bar{\eta}}$$

$$\frac{\partial^2}{\partial x \partial y} = \frac{1}{\cos \alpha} \frac{\partial^2}{\partial \bar{\xi} \partial \bar{\eta}} - \frac{\tan \alpha}{R} \frac{\partial^2}{\partial \bar{\eta}^2}$$

$$dx \, dy = \cos \alpha \, d\bar{\xi} \, d\bar{\eta} \tag{24}$$

Make the following non-dimensionalizations,

$$\eta = \bar{\eta}/\gamma$$

$$\xi = \bar{\xi}/\ell \tag{25}$$

where γ is the half-angle at $\xi = 0$, and ℓ is the slant length (see Fig. 4). Substitution of Eq. (25) into Eq. (24) yields,

$$\frac{\partial}{\partial x} = \frac{1}{\ell \cos \alpha} \frac{\partial}{\partial \xi} - \frac{\tan \alpha}{\gamma R} \frac{\partial}{\partial \eta}$$

$$\frac{\partial}{\partial y} = \frac{1}{\gamma} \frac{\partial}{\partial \eta}$$

$$\frac{\partial^2}{\partial y^2} = \frac{1}{\gamma^2} \frac{\partial^2}{\partial \eta^2}$$

$$\frac{\partial^2}{\partial x^2} = \frac{1}{\ell^2 \cos^2 \alpha} \frac{\partial^2}{\partial \xi^2} + \frac{\tan^2 \alpha}{R^2 \gamma^2} \frac{\partial^2}{\partial \eta^2} - \frac{2 \tan \alpha}{R \gamma \ell \cos \alpha} \frac{\partial^2}{\partial \xi \partial \eta}$$

$$\frac{\partial^2}{\partial x \partial y} = \frac{1}{\ell \cos \alpha} \frac{1}{\gamma} \frac{\partial^2}{\partial \xi \partial \eta} - \frac{\tan \alpha}{R \gamma^2} \frac{\partial^2}{\partial \eta^2}$$

$$dx \, dy = \ell \gamma \cos \alpha \, d\xi \, d\eta \tag{26}$$

Case of the Parallelogram

When the projection of the open circular shell in Fig. 4 is a parallelogram (a helicoidal shell), the foregoing coordinate transformation will yield constant limits on the integrals in the energy equations [Eqs. (19) - (21)] and thus facilitate exact integration. Assuming a helicoidal shell with constant thickness h, the following equations result from substituting Eq. (26) into Eqs. (19)-(21).

$$
\begin{aligned}
\int_{-1}^{1} \int_{0}^{1} &\Big\{ [u_\xi \ \delta u_\xi + (\sin^2\alpha + \frac{(1-\nu)}{2}\cos^2\alpha)(\ell/R\gamma)^2 u_\eta \ \delta u_\eta \\
&- \sin\alpha \ (\ell/R\gamma)(u_\eta \ \delta u_\xi + u_\xi \ \delta u_\eta)] + (\ell/R\gamma) \cdot \\
&[\frac{(1-\nu)}{2}\cos\alpha \ v_\xi \ \delta u_\eta + \nu \cos\alpha \ v_\eta \ \delta u_\xi - (\ell/R\gamma) \cdot \\
&(\sin\alpha)(\cos\alpha)\frac{(1+\nu)}{2} v_\eta \ \delta u_\eta] + [(\ell/R) \ \nu \cos\alpha \ w \ \delta u_\xi \\
&- (\ell/R)(\ell/R\gamma) \ \nu \cos\alpha \sin\alpha \ w \ \delta u_\eta] \\
&- \omega^2 \frac{\rho}{E}(1-\nu^2)\ell^2\cos^2\alpha \ [u \ \delta u] \Big\} d\xi \ d\eta = 0
\end{aligned}
\tag{27}
$$

$$\int_{-1}^{1}\int_{0}^{1} \left\{ (\ell/R\gamma)\left[\frac{(1-\nu)}{2}\cos\alpha \ u_\eta \ \delta v_\xi + \nu \cos\alpha \ u_\xi \ \delta v_\eta \right. \right.$$

$$\left. - (\ell/R\gamma)(\sin\alpha)(\cos\alpha)\frac{(1+\nu)}{2} u_\eta \ \delta v_\eta \right]$$

$$+ \left[1 + (h/R)^2/12\right]\left[(\ell\cos\alpha/R\gamma)^2 \ v_\eta \ \delta v_\eta \right]$$

$$+ \left[1 + (h/R)^2/3\right]\frac{(1-\nu)}{2}\left[(\ell\sin\alpha/R\gamma)^2 \ v_\eta \ \delta v_\eta \right.$$

$$\left. + v_\xi \ \delta v_\xi - (\ell\sin\alpha/R\gamma)(v_\eta \ \delta v_\xi + v_\xi \ \delta v_\eta)\right]$$

$$+ \left[(\ell\cos\alpha/R)^2 \frac{1}{\gamma} w \ \delta v_\eta \right] - \left[(h/R)^2/12\gamma\right] \cdot$$

$$\left[(\ell/R\gamma)^2(1 + (1-\nu)\sin^2\alpha)w_{\eta\eta} \ \delta v_\eta + \nu \ w_{\xi\xi} \ \delta v_\eta \right.$$

$$- 2(\ell/R\gamma)\sin\alpha \ w_{\xi\eta} \ \delta v_\eta + 2(1-\nu) \ w_{\xi\eta} \ \delta v_\xi$$

$$\left. - 2(1-\nu)(\ell/R\gamma)\sin\alpha \ w_{\eta\eta} \ \delta v_\xi \right]$$

$$\left. - \omega^2 \frac{\rho}{E}(1-\nu^2)\ell^2\cos^2\alpha \left[v \ \delta v\right]\right\} d\xi \ d\eta = 0 \tag{28}$$

$$
\int_{-1}^{1}\int_{0}^{1} \left\{ (\ell/R) \left[\nu \cos\alpha \ u_\xi \ \delta w - (\ell/R\gamma) \nu \cos\alpha \sin\alpha \ u_\eta \ \delta w \right] \right.
$$

$$
+ \frac{1}{\gamma}(\ell\cos\alpha/R)^2 \left[v_\eta \ \delta w \right] - \left[(h/R)^2/12\gamma \right] \cdot
$$

$$
\left[(\ell/R\gamma)^2 (1 + (1-\nu)\sin^2\alpha) \ v_\eta \ \delta w_{\eta\eta} + \nu \ v_\eta \ \delta w_{\xi\xi} \right.
$$

$$
- 2(\ell/R\gamma) \sin\alpha \ v_\eta \ \delta w_{\xi\eta} + 2(1-\nu) \ v_\xi \ \delta w_{\xi\eta}
$$

$$
\left. - 2(1-\nu)(\ell/R\gamma) \sin\alpha \ v_\xi \ \delta w_{\eta\eta} \right] + \left[(\ell\cos\alpha/R)^2 \ w \ \delta w \right]
$$

$$
+ \left[(h/R)^2/12 \right] \left[(R/\ell\cos\alpha)^2 \ w_{\xi\xi} \ \delta w_{\xi\xi} + (\ell/R\gamma^2\cos\alpha)^2 \cdot \right.
$$

$$
w_{\eta\eta} \ \delta w_{\eta\eta} + \frac{1}{\gamma^2} (\tan^2\alpha + \nu)(w_{\eta\eta} \ \delta w_{\xi\xi} + w_{\xi\xi} \ \delta w_{\eta\eta})
$$

$$
+ \frac{1}{\gamma^2} (2(1-\nu) + 4\tan^2\alpha) \ w_{\xi\eta} \ \delta w_{\xi\eta} - 2(\ell/R\gamma) \frac{1}{\gamma^2} \cdot
$$

$$
\frac{\tan\alpha}{\cos\alpha} (w_{\eta\eta} \ \delta w_{\xi\eta} + w_{\xi\eta} \ \delta w_{\eta\eta}) - 2 \frac{\tan\alpha}{\cos\alpha} (R/\gamma\ell) \cdot
$$

$$
\left. (w_{\xi\xi} \ \delta w_{\xi\eta} + w_{\xi\eta} \ \delta w_{\xi\xi}) \right] - \omega^2 \frac{\rho}{E}(1-\nu^2)\ell^2\cos^2\alpha \left[w \ \delta w \right]
$$

$$
\left. \right\} d\xi \ d\eta = 0 \tag{29}
$$

14

For the limiting case of the flat plate in bending, Eq. (29) reduces to the following;

$$\int_{-1}^{1} \int_{0}^{1} \left[w_{\xi\xi} \, \delta w_{\xi\xi} + (\ell/b)^4 \, w_{\eta\eta} \, \delta w_{\eta\eta} \right.$$

$$+ (\sin^2\alpha + \nu \cos^2\alpha)(\ell/b)^2 (w_{\eta\eta} \, \delta w_{\xi\xi} + w_{\xi\xi} \, \delta w_{\eta\eta})$$

$$+ [2(1-\nu)\cos^2\alpha + 4 \sin^2\alpha)(\ell/b)^2 (w_{\xi\eta} \, \delta w_{\xi\eta})$$

$$- 2(\ell/b)^3 \sin\alpha \, (w_{\eta\eta} \, \delta w_{\xi\eta} + w_{\xi\eta} \, \delta w_{\eta\eta})$$

$$- 2(\ell/b) \sin\alpha \, (w_{\xi\xi} \, \delta w_{\xi\eta} + w_{\xi\eta} \, \delta w_{\xi\xi})$$

$$\left. - \omega^2 \, \frac{\rho}{E} \, 12(1-\nu^2) \, \frac{\ell^4}{h^2} \cos^4\alpha \, w \, \delta w \right] d\xi \, d\eta = 0 \qquad (30)$$

where ℓ is the slant length of the plate and b is the half-width (see Fig. 2).

SOLUTIONS

Boundary Conditions

As is well known [2], one need only satisfy geometric boundary conditions when using the Ritz method with displacement energy equations. For a cantilever boundary, the geometric boundary conditions are,

$$u = 0 \text{ at } x = 0 \text{ for all } y$$

$$v = 0 \text{ at } x = 0 \text{ for all } y$$

$$w = 0 \text{ at } x = 0 \text{ for all } y$$

$$w_x = 0 \text{ at } x = 0 \text{ for all } y \tag{31}$$

From Eqs. (22) and (25) it follows that $x = 0$ implies $\xi = 0$. Eq. (26) and the last of Eq. (31) gives,

$$w_x = \frac{1}{\ell\cos\alpha} w_\xi - \frac{\tan\alpha}{R\gamma} w\eta = 0 \text{ at } x = \xi = 0$$
$$\text{for all } y \text{ and } \eta \tag{32}$$

or,

$$w_x = \frac{1}{\ell\cos\alpha} w_\xi - \frac{\tan\alpha}{R} w_y = 0 \text{ at } x = \xi = 0$$
$$\text{for all } y \tag{32}$$

But since $w = 0$ at $x = 0$ for all y, $w_y = 0$ at $x = 0$ for all y as a result. Thus in terms of the skewed coordinates ξ and η, Eqs. (31) and (32) become,

$$u = 0 \text{ at } \xi = 0$$

$$v = 0 \text{ at } \xi = 0$$

$$w = 0 \text{ at } \xi = 0$$

$$w_\xi = 0 \text{ at } \xi = 0 \tag{33}$$

Assumed Functions

Using the concepts set forth in Ref. [15], direct solutions to conservative, non-conservative, stationary, and non-stationary systems of particles, rigid bodies, beams, plates, and shells have been obtained with nothing more than power series in Eq. (2). It has been the author's experience that they also give more accurate answers than beam functions for plate and shell vibration problems (beam functions place unnecessary constraints on higher derivatives at plate and shell boundaries for some boundary conditions).

The geometric boundary conditions [Eq. (33)] dictate the following double power series.

$$u = \sum_{i=0}^{N} \sum_{j=0}^{M} A_{ij} \, \xi^{i+1} \, \eta^{j}$$

$$v = \sum_{i=0}^{N} \sum_{j=0}^{M} B_{ij} \, \xi^{i+1} \, \eta^{j}$$

$$w = \sum_{i=0}^{N} \sum_{j=0}^{M} C_{ij} \, \xi^{i+2} \, \eta^{j} \tag{34}$$

Eigenvalue Equations

The δ operator in Eqs. (27)–(30) now has the following definitions [5],

$$\delta u = \frac{\partial u}{\partial A_{k\ell}} \, \delta A_{k\ell} = \xi^{k+1} \, \eta^{\ell} \, \delta A_{k\ell}$$

$$\delta v = \frac{\partial v}{\partial B_{k\ell}} \, \delta B_{k\ell} = \xi^{k+1} \, \eta^{\ell} \, \delta B_{k}$$

$$\delta w = \frac{\partial w}{\partial C_{k\ell}} \, \delta C_{k\ell} = \xi^{k+2} \, \eta^{\ell} \, \delta C_{k} \tag{35}$$

where $\delta A_{k\ell}$, $\delta B_{k\ell}$, and $\delta C_{k\ell}$ are arbitrary quantities (or "variations"), which may be factored out of Eqs. (27)–(30).

Upon substitution of Eqs. (34) and (35) into Eqs. (27)-(29), the following coupled algebraic equations result;

$$\sum_{i=0}^{N} \sum_{j=0}^{M} \left\{ A_{ij} [K1_{ijk\ell} - \lambda_s^2 M1_{ijk\ell}] + B_{ij} K2_{ijk\ell} \right.$$

$$\left. + C_{ij} K3_{ijk\ell} \right\} = 0 \qquad \text{for } k = 0,1...,N$$
$$\ell = 0,1...,M \qquad (36)$$

$$\sum_{i=0}^{N} \sum_{j=0}^{M} \left\{ A_{ij} K2_{k\ell ij} + B_{ij} [K4_{ijk\ell} - \lambda_s^2 M2_{ijk\ell}] \right.$$

$$\left. + C_{ij} K5_{ijk\ell} \right\} = 0 \qquad \text{for } k = 0,1...,N$$
$$\ell = 0,1...,M \qquad (37)$$

$$\sum_{i=0}^{N} \sum_{j=0}^{M} \left\{ A_{ij} K3_{k\ell ij} + B_{ij} K5_{k\ell ij} + C_{ij} [K6_{ijk\ell} \right.$$

$$\left. - \lambda_s^2 M3_{ijk\ell}] \right\} = 0 \qquad \text{for } k = 0,1...,N$$
$$\ell = 0,1...,M \qquad (38)$$

where $K1_{ijk\ell}$, $K2_{ijk\ell}$, $K3_{ijk\ell}$, $K4_{ijk\ell}$, $K5_{ijk\ell}$, $K6_{ijk\ell}$, $M1_{ijk\ell}$, $M2_{ijk\ell}$ and $M3_{ijk\ell}$ are given in Appendix II in terms of recurrsion formulas which result from exact integration. Eqs. (36)-(38) form a set of $3 \times (N+1) \times (M+1)$ algebraic equations in the $(3 \times (N+1) \times (M+1)) + 1$ unknown A_{ij}'s, B_{ij}'s, C_{ij}'s, and λ_s^2 ($\equiv \omega^2 \frac{\rho}{E} (1-\nu^2)\ell^2\cos^2\alpha$). They are conveniently written in the following matrix form;

$$\left\{ \begin{bmatrix} K1 & K2 & K3 \\ K2^T & K4 & K5 \\ K3^T & K5^T & K6 \end{bmatrix} - \lambda_s^2 \begin{bmatrix} M1 & 0 & 0 \\ 0 & M2 & 0 \\ 0 & 0 & M3 \end{bmatrix} \right\} \begin{bmatrix} A \\ B \\ C \end{bmatrix} = 0 \qquad (39)$$

For a non-trivial solution, the determinant of the coefficient matrix must vanish.

The Skewed Plate

The limiting case of the flat plate in bending, using Eqs. (34), (35), and (30), yields the following eigenvalue equation:

$$\sum_{i=0}^{N} \sum_{j=0}^{M} C_{ij} [KB_{ijk\ell} - \lambda_p^2 M3_{ijk\ell}] = 0$$

$$\text{for } K = 0,1,2,\ldots,N$$

$$\ell = 0,1,2,\ldots,M \qquad (40)$$

or in matrix form,

$$\{[KB] - \lambda_p^2[M3]\} \; \{C\} = 0 \qquad (41)$$

$KB_{ijk\ell}$ is given in Appendix II. Eq. (41) is a set of (N+1) X (M+1) algebraic equations in the (N+1) X (M+1) + 1 unknown C_{ij}'s and $\lambda_p^2 (\equiv \omega^2(\rho h/D)\ell^4 \cos^4\alpha)$. Again, to have a non-trivial solution, the determinant of the coefficient matrix in Eq. (41) must vanish.

CHAPTER III. .

RESULTS

The Skewed Plate

For the sake of completeness (since the flat plate is
the limiting case of the helicoidal shell being considered)
and due to the relatively small amount of attention given
the skewed cantilever plate in the literature, plate eigen-
values and mode shapes for various aspect ratios and skew
angles will be presented. Comparisons of the present solu-
tion with other analytical and experimental results will be
given for the skewed plate.

Four aspect ratios (AR = $\ell/2b$) are considered: 0.5, 1.0,
2.0, 4.0. Poisson's ratio is set to a nominal value of 0.3
for all plate calculations. Also α is restricted to 0°, 15°,
30°, and 45°. Permissible ranges are $0 < AR < \infty$ and $0° \leq \alpha < 90°$.
The authors have made unverified calculations for α up to 85°
without any difficulty. However, those results will not be
included since the helicoidal shell data was restricted to
$0° \leq \alpha \leq 45°$. The values chosen for AR and α yield 16 possible
parameter combinations. All calculations used a 35 term double
power series for w. No loss of numerical accuracy (16 place
arithmetic was used) was apparent for the 35 x 35 matrix eigen-
value problem. As α increases, the coupling between odd and
even η terms increases, causing the computation of the eigen-
values to take longer. The total cost of the 16 eigenvalue
problems was $20.00 on the IBM 370 digital computer. Conver-
gence curves will not be given since only the 5 lowest modes
of each parameter combination will be given. For 35 terms,
the 5 lowest modes are converged (throughout the text the word
"converged" means that less than 0.5% change occurred in the
eigenvalues when additional terms were taken in the double
power series).

Table 1 contains the 5 lowest eigenvalues for all 16
parameter combinations. For the data given in Table 1, eigen-
value curves may be plotted versus α, since the eigenvalues
are continuous functions of α. Plots of the eigenvalues versus
α for AR = 0.5, 1.0, 2.0, and 4.0 appear in Figs. 5, 6, 7, and
8 respectively. For AR = 0.5 and 4.0 (Figs. 5 and 8) no mode
crossing can be detected for $0° \leq \alpha \leq 45°$ although nodal
patterns are altered with increasing α (see Figs. 9, 10, 11,
and 12). For AR = 1.0, Fig. 6 shows the 3rd and 4th mode
shapes reversing their order at very nearly $\alpha = 32°$. Also
the 5th and 6th mode shapes reverse position at $\alpha = 38°$. Thus
one frequency must generate 2 independent mode shapes at points
of intersection of 2 curves (i.e., at some precise α value).
These reversals of position in the frequency spectrum of a
given mode shape can be evidenced in the w nodal patterns
(Figs. 9-12). For AR = 2.0 only the 5th and 6th mode shapes
cross (nearly at $\alpha = 41°$). As aspect ratio increases, a given

nodal pattern may drastically change its position in the
frequency spectrum (see Figs. 9-12). This is due to the
fact that as AR decreases the relative longitudinal stiff-
ness increases, thus causing more of the lower modes to have
longitudinal nodal lines.

Tables 2 and 3 contain comparisons of these power
series results to experimental and other analytical results.
Aspect ratio is 1.0 in both tables.

$$\alpha = 30° \text{ (Table 2)}$$

Column 1 contains experimental results from References
[11] and [12]. Column 2 contains the authors' direct solu-
tion. Column 3 has analytical results due to Claassen [13],
who used 18 beam functions in a Ritz analysis. Note that
Claassen's results are all higher than the author's direct
solution. Since the Ritz method yields upper bounds, the
author's numbers are more converged than Claassen's [13] re-
sults. Column 4 contains experimental results given in
Reference [14]. The agreement between analysis and experi-
ment is very good considering that in some instances, shakers
were used to excite the plate (shaker position can drasti-
cally affect mode shapes and thus nodal patterns, as evidenced
in Ref. [14]).

$$\alpha = 45° \text{ (Table 3)}$$

Columns 1, 2, and 4 are the same as in Table 2. Column
3 contains analytical results obtained using Reissner's
theorem [15]. In light of the experimental data in Columns
1 and 4, and the well converged (less than 0.5% error) analy-
tical results in Column 2, some of the results in Column 3
are upper bounds and some are lower bounds. Again the
analytical results in Column 2 agree favorably with the experi-
mental results.

THE HELICOIDAL SHELL

Since there is no data for comparison to the cantilever helicoidal shell, convergence of the eigenvalues must be checked to establish their validity. In choosing the three double power series, no preference is made for u, v, or w. All three double power series are given the same number and degree terms. For large aspect ratio higher order ξ terms are needed, whereas for smaller aspect ratios higher order η terms are needed. 16 place arithmetic is used throughout the calculations. For the largest number of terms taken (30 terms in each series; a 90 x 90 matrix eigenvalue problem) no loss of accuracy was noted.

First a simple configuration (ℓ/R = 0.2, h/R = 0.01, α = 0°, and γ = 0.1 rad) was checked. For the helicoidal shell aspect ratio is AR = $\ell/2R\gamma$. In this particular case AR = 1.0. Convergence curves for the first 5 eigenvalues appear in Fig. 13. The first 4 modes are converged after only 16 terms (48 x 48 matrix) and all 5 are converged at 24 terms (72 x 72 matrix). Next, the same shell with α = 45° was checked. The convergence curves are given in Fig. 14. For 24 terms all 5 eigenvalues are very close (within 1.5%) to the converged numbers of 30 terms. As a last example, an aspect ratio 4.0 shell (ℓ/R = 0.8, h/R = 0.01, α = 15° and γ = 0.1 rad) was checked. Convergence curves are shown in Fig. 15. Again 24 terms yield results within 2% of the converged numbers of 30 terms. Convergence of other examples, such as small aspect ratio (large γ), have been checked but will not be included, since the results are virtually the same as the three cases presented. Of course it would be desirable to run all cases with 30 terms to assure converged numbers. For a 24 term run (72 x 72 matrix), the average cost on the IBM 370 digital computer was $10.00. Thus, as a matter of economy, and in order to present the widest range of data possible, all results presented will be for 24 or 25 terms. As has been shown, the eigenvalues for 24 terms are within 2% of the converged numbers of 30 terms.

The geometric parameters are ℓ/R, h/R, α and γ. Poisson's ratio was set to a nominal value of 0.3 for all calculations. For thin shell theory h/R is usually taken in the range $0 < h/R \leq 0.05$. This is in keeping with the approximations made in the derivation of the thin shell equations. In this paper only h/R in the range $0.005 \leq h/R \leq 0.05$ will be considered. Also α will be restricted to $0 \leq \alpha \leq \pi/4$ and γ to 0.1 rad $\leq \gamma \leq 0.7$ rad. Permissible ranges for α and γ are of course $0 \leq \alpha \leq \pi/2$

and $0 < \gamma \le \pi$. The permissible range for ℓ/R is $0 < \ell/R < \infty$. But again, in order to limit the enormous amount of possible parameter combinations, ℓ/R is taken in the range $0.1 < \ell/R \le 0.8$. In order to observe the effects of a given parameter, all other parameters are fixed at values which could represent a typical shell.

Effect of h/R

For $\alpha = 0°$; $\ell/R = 0.2$; $\gamma = 0.1$ rad

The aspect ratio for this case is 1.0. For small R/h (= 20), the primarily bending modes (denoted by B_1, B_2,...) have relatively high frequencies. Also one encounters primarily membrane modes (denoted by M_1, M2,...) much earlier in the spectrum. But as R/h increases, the frequencies of the primarily bending modes decreases rapidly (see Fig. 16). Since the frequencies of the primarily membrane modes change very little with R/h, they appear later and later in the spectrum due to the rapid decrease in the bending mode eigenvalues.

For $\alpha = 30°$, $\ell/R = 0.2$; $\gamma = 0.1$ rad

The trend of the eigenvalues versus R/h remains the same with this change in α (see Fig. 17). The eigenvalue for the M_1 mode is consistantly lower for $\alpha = 30°$ than for $\alpha = 0°$. Also the eigenvalues for B_4 and B_5 are consistantly lower for $\alpha = 30°$ than for $\alpha = 0°$. For $\alpha = 30°$, modes B_3 and B_4 are very close in frequency versus R/h, although the mode shapes differ considerably.

Effect of α

For $\ell/R = 0.2$; h/R = 0.01; $\gamma = 0.1$ rad

The aspect ratio is 1.0. Table 4 contains the first 5 eigenvalues for $\alpha = 0°$, 15°, 30°, and 45°. Also included are the relative amounts of bending strain energy and membrane strain energy, and the generalized mass. The eigenfunctions were normalized in such a way as to make the generalized mass be between 1.0 and 10.0. The generalized stiffness (total strain energy) is then λ_s^2 X generalized mass. The generalized mass and stiffness would be used in calculating transient motion of the shell by the normal coordinate technique. If a mode has more than 60% of the strain energy due to membrane energy, it is considered a primarily membrane mode, denoted by M. If more than 60% of the strain energy is due to bending, it is considered a primarily bending mode, denoted by B.

If neither is more than 60%, the mode is denoted by B-M or M-B, the first letter indicating which is greater in magnitude. Eigenvalues will not be graphed versus the remaining geometric parameters. This is because mode shapes and frequencies change rapidly and it becomes very difficult to draw curves for the 5 lowest modes. Rather, the 5 lowest eigenvalues will be given in tabular form along with figures showing the w nodal patterns. For the present case, w nodal patterns appear in Fig. 16. The 1st and 2nd mode shapes can be easily followed versus α. The 3rd and 4th modes, however, cross between α = 30° and 45°. Also between 30° and 45°, a bending mode crosses a membrane mode (5th mode).

For ℓ/R = 0.8; h/R = 0.01; γ = 0.1 rad

The aspect ratio is 4.0. Eigenvalues and energy percentages are given in Table 5. In Fig. 19 the first 3 modes can easily be followed versus α. However, the 4th and 5th modes are difficult to follow. At α = 15°, the 4th and 5th mode w nodal patterns are very nearly the same. Yet, the relative magnitudes and/or shapes of u and v may be entirely different. This fact will be illustrated in a later section. After α = 15°, the 4th and 5th modes seem to retain their position in the frequency spectrum.

Effect of γ

For ℓ/R = 0.8, h/R = 0.01; γ = 0°

The aspect ratio varies with γ (AR = ℓ/2Rγ). Eigenvalues and strain energy percentages are given in Table 6. w nodal patterns appear in Fig. 20. For γ = 0.1 rad, the w nodal patterns are very similar to those for the flat plate. As γ increases, the relative longitudinal stiffness increases causing two things to occur: first, more longitudinal node lines appear in the lower modes, and second, the membrane energy for the lower modes increases considerably. It is almost impossible to follow a given nodal pattern versus γ. Although one or two deflection components may have the same (or similar) nodal patterns for different nodes, the third component may have a very different nodal pattern for the two modes. This is illustrated by modes 2 and 3 for γ = 0.7 rad. Even though the w nodal patterns are different, u and v have similar nodal patterns (see Fig. 21). The relative magnitudes of u, v, and w are also similar for the two modes shown in Fig. 21. Upon close inspection, although u and v nodal lines are similar, their positioning is different.

For $\ell/R = 0.8$; $h/R = 0.01$; $\alpha = 30°$

Aspect ratio varies with γ as noted before. Eigenvalues and strain energy percentages are given in Table 7. w nodal patterns are shown in Fig. 22. Modes 1, 2, and 3 seem to follow an orderly progression from $\gamma = 0.1$, 0.3, 0.5, to 0.7, with each increase in γ bringing an additional longitudinal node line. As previously mentioned, this is a result of the relative increase of the longitudinal stiffness. Modes 4 and 5 are difficult to follow. Mode 4 seems to follow the trend of increasing number of longitudinal node lines with increasing γ. At $\gamma = 0.5$ rad, modes 4 and 5 have similar w nodal patterns; but, u and v nodal patterns may be quite different.

Effect of ℓ/R

For $h/R = 0.01$; $\alpha = 0$; $\gamma = 0.1$ rad

The aspect ratio (AR = $\ell/2R\gamma$) varies since ℓ/R varies. Eigenvalues and strain energy percentages are shown in Table 10. w nodal patterns are shown in Fig. 23. Unfortunately, Fig. 23 is somewhat distorted. γ is fixed at 0.1 rad, so as ℓ/R decreases, the length of the planforms should decrease. Instead, the length of the planform has been fixed at one unit and the width ($2\gamma R/\ell$) thus increases as ℓ/R decreases. Except for one membrane mode each in $\ell/R = 0.8$ and 0.4, all other modes shown are primarily bending modes. As AR decreases (ℓ/R decreasing), the relative longitudinal stiffness increases, with the result that more of the lower modes have longitudinal node lines. Notice the similarity in Fig. 23 and the analogous flat plate in Fig. 9. The w nodal patterns are identical with the exceptions of mode 5 for AR = 2.0 and modes 4 and 5 for AR = 4.0.

For $h/R = 0.01$; $\alpha = 30°$; $\gamma = 0.1$ rad

Again the aspect ratio varies with ℓ/R. Eigenvalues and strain energy percentages are given in Table 9. w nodal patterns are shown in Fig. 24. Fig. 24 has the same distortions as Fig. 23. The 1st and 2nd modes can be followed easily as AR decreases (ℓ/R decreasing). As before, more of the lower modes have longitudinal nodal lines as AR decreases. Note the similarity to the flat plate nodal patterns (Fig. 11). The reason for the similarity is the shallowness ($\gamma = 0.1$ rad) of this particular shell.

CONCLUDING REMARKS

Free vibration modes and frequencies have been presented for both the cantilever skewed plate and cantilever helicoidal shell with variations of all geometric parameters. From the convergence curves in the case of the shell, and from experimental and other analytical results in the case of the plate, the authors feel that the results are numerically sound.

The shell results point up the serious problems which confront the designer. That is the question of what the first few mode shapes are. It is impossible (especially for large γ in the case of the shell) to guess at the mode shapes in order to get a 1 or 2 term Rayleigh-Ritz solution that will yield anything close to the true fundamental frequency. In short, anticipating the mode shapes of the helicoidal shell is not feasible. As R/h increases, the spacing between shell eigenvalues rapidly decreases, causing mode excitation, identification, and resolution to be very difficult for the experimentalist. Also as α and γ increase, nodal patterns change drastically, thus furthering the problem of mode identification. At some α values two mode shapes exist for one frequency, for both the plate and shell. Positions of given nodal patterns in the frequency spectrum are altered drastically with changes in aspect ratio for the plate and shell.

It is felt that this paper represents a third step toward the analytical solution to the flutter of the thermally stressed turbine blade. The first and second steps are represented in Refs. 2 and 16 respectively. The turbine blade, immersed in a non-steady fluid flow field and a non-steady structural acceleration field, poses a challenging problem for an analytical solution. The Ritz method, when power series are properly employed with finite time intervals and finite space intervals in Hamilton's Law of Varying Action, appears to offer a direct method of attack on this and other most difficult problems.

## COMPARISON TO EXACT SOLUTIONS FOR SPHERICAL CAPS AND THE COMPLETE CONICAL SHELL

A literature search was made including the Applied Mechanics Reviews, Index to Contemporary Acoustical Literature published by the Acoustical Society of America, a computer survey from NASA Langley Research Center, and the NASA monographs, "Vibration of Plates" and "Vibration of Shells" by A. W. Leissa [1], [17]. No exact solution exists for the skewed cantilever plate or for the cantilevered helicoidal shell [17]. No numerical results from either calculation or experiment, were found in the literature on the vibration modes and frequencies of the cantilevered helicoidal shell. However, comparison of calculations by the authors, using power series, have been made to the "exact" solutions for two other shell geometries and are given below.

The Deep Spherical Shell

The exact solution for the deep spherical shell is given in terms of Legendre functions of the first kind by Kalnins [18] and Kraus [19]. In the exact solution, $(h/R)^2/12$ has been neglected in comparison to unity, in order to arrive at a solvable differential equation (this is in keeping with the approximations made in thin shell theory). In the present analysis $(h/R)^2/12$ was retained.

For axisymmetric motion (i.e., only u and w deflections present), Kalnins [18] has given eigenvalues for various boundary conditions. In the direct solution by the authors, a 10 term power series was used for both u and w. A comparison of results for a clamped base and a free base is given in Table 1 of this Appendix. The agreement is quite evident. The reason the direct solution (shown by Ritz [4] to be an upper bound for stationary problems) yields a lower eigenvalue for the first few modes than the exact solution, is felt to be that the differential equations that would be obtained from the energy equation are slightly different than the differential equations of Ref. [17] due to the neglect of $(h/R)^2/12$ in comparison to unity.

TABLE 1. DEEP SPHERICAL SHELL
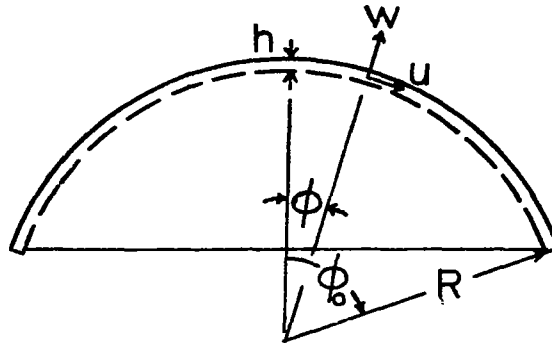
Axisymmetric Motion

$h/R = 0.05$, $\nu = 0.3$, $\phi_o = 60°$		
$\lambda^* = \omega R\sqrt{\rho/E}$		
Mode No.	Free Base	Clamped Base
1	0.931[a] [0.9308][b]	1.006 [1.0056]
2	1.088 [1.088]	1.391 [1.391]
3	1.533 [1.5336]	1.697 [1.6963]
4	2.348 [2.3488]	2.375 [2.3746]
5	2.544 [2.5478]	3.486 [3.4872]
6	3.497 [3.5346]	3.991 [3.9907]
7	4.951 [5.0956]	4.974 [4.9792]

a. unbracketed numbers due to Kalnins [18]
b. [ ],bracketed numbers from author's direct solution

28

The Complete Cone

Due to the geometric singularities at the apex, the complete conical shell has received little treatment by the Ritz method, and limited exact solution. Neglecting tangential inertia ($\ddot{u} = 0$), an exact solution has been obtained by using Airy's stress function and the method of Frobenius [20]. Dreher [20] used the Donnell-Mushtari shell equations. The author used Novozhilov's strain-displacement relations to obtain the direct solution of the free base case, with and without tangential inertia. Reference [20] gave numerical results for the clamped and free base. A comparison of results is given in Table 2 of this Appendix. The small difference in the frequencies from the exact solution and the direct solution, when tangential inertia was neglected, is probably due to the fact that slightly different equations were solved. The result of neglecting tangential inertia has the predictable effect of raising the natural frequencies since mass is effectively taken out of the system (or conversely, constraints have been added).

TABLE 2. CONICAL SHELL
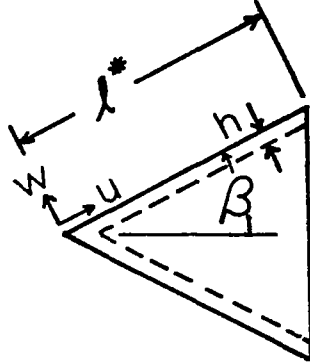
Axisymmetric Motion		
$\ell^* = 24.25$	$\rho = 0.000254 \, \text{lb-sec}^2/\text{in}^4$	
$\nu = 0.3$	$\beta = 60°$	
$E = 10^7 \, \text{psi}$	$N^* = 12(1-\nu^2)(\ell^*/h)^2/\tan^2\beta$	
$h = 0.4626 \, \text{in}$	$= 10^4$	

Frequency, Hz		

Mode No.	Neglecting $\ddot{u}$		Including $\ddot{u}$
	Exact Solution, Ref. [20]	Direct Solution, author	Direct Solution, author
1	912.36	912.35	891.47
2	1322.53	1322.60	1269.34
3	1823.71	1828.55	1746.54
4	2414.92	2410.31	2310.01
5	3122.80	3264.53	2987.97

APPENDIX II

MATRIX ELEMENTS

for $(i+\ell)$

$$I1_{ijk\ell} = 0 \qquad\qquad\qquad \text{odd}$$

$$= 2\,\frac{(i+1)(k+1)}{i+k+1}\;\frac{1}{j+\ell+1} \qquad \text{even}$$

$$I2_{ijk\ell} = 0 \qquad\qquad\qquad \text{odd}$$

$$= 2\,\frac{1}{i+k+3}\;\frac{j\ell}{j+\ell-1} \qquad \text{even}$$

$$I3_{ijk\ell} = 2\,\frac{(k+1)j+\ell(i+1)}{(i+k+2)(j+\ell)} \qquad \text{odd}$$

$$= 0 \qquad\qquad\qquad \text{even}$$

$$I4_{ijk\ell} = 2\,\frac{\ell(i+1)}{(i+k+2)(j+\ell)} \qquad \text{odd}$$

$$= 0 \qquad\qquad\qquad \text{even}$$

$$I5_{ijk\ell} = 2\,\frac{j(k+1)}{(i+k+2)(j+\ell)} \qquad \text{odd}$$

$$= 0 \qquad\qquad\qquad \text{even}$$

$$I6_{ijk\ell} = 0 \qquad\qquad\qquad \text{odd}$$

$$= 2\,\frac{1}{(i+k+3)}\;\frac{j\ell}{j+\ell-1} \qquad \text{even}$$

31

$$I7_{1jkl} = 0 \qquad\qquad \text{odd}$$

$$= 2 \frac{(k+1)}{(1+k+3)} \frac{1}{(j+l+1)} \qquad \text{even}$$

$$I8_{1jkl} = 2 \frac{1}{(1+k+4)} \frac{l}{(j+l)} \qquad \text{odd}$$

$$= 0 \qquad\qquad \text{even}$$

$$I9_{1jkl} = 2 \frac{1}{(1+k+4)} \frac{j(j-1)l}{(j+l-2)} \qquad \text{odd}$$

$$= 0 \qquad\qquad \text{even}$$

$$I10_{1jkl} = 2 \frac{(1+2)(1+1)}{(1+k+2)} \frac{l}{(j+l)} \qquad \text{odd}$$

$$= 0 \qquad\qquad \text{even}$$

$$I11_{1jkl} = 0 \qquad\qquad \text{odd}$$

$$= 2 \frac{(1+2)}{(1+k+3)} \frac{jl}{(j+l-1)} \qquad \text{even}$$

$$I12_{1jkl} = 2 \frac{(1+2)(k+1)}{(1+k+2)} \frac{j}{(j+l)} \qquad \text{odd}$$

$$= 0 \qquad\qquad \text{even}$$

$$I13_{1jkl} = 0 \qquad\qquad \text{odd}$$

$$= 2 \frac{(k+1)}{(1+k+3)} \frac{j(j-1)}{(j+l-1)} \qquad \text{even}$$

$$I14_{ijk\ell} = 0 \qquad\qquad \text{odd}$$

$$= 2\,\frac{1}{(i+k+5)}\,\frac{1}{(j+\ell+1)} \qquad \text{even}$$

$$I15_{ijk\ell} = 0 \qquad\qquad \text{odd}$$

$$= 2\,\frac{(i+2)(i+1)(k+2)(k+1)}{(i+k+1)(j+\ell+1)} \qquad \text{even}$$

$$I16_{ijk\ell} = 0 \qquad\qquad \text{odd}$$

$$= 2\,\frac{j(j-1)\ell(\ell-1)}{(i+k+5)(j+\ell-3)} \qquad \text{even}$$

$$I17_{ijk\ell} = 0 \qquad\qquad \text{odd}$$

$$= 2\,\frac{(i+2)(i+1)\ell(\ell-1)+(k+2)(k+1)j(j-1)}{(i+k+3)(j+\ell-1)}$$
$$\text{even}$$

$$I18_{ijk\ell} = 0 \qquad\qquad \text{odd}$$

$$= 2\,\frac{(i+2)(k+2)j\ell}{(i+k+3)(j+\ell-1)} \qquad \text{even}$$

$$I19_{ijk\ell} = 2\,\frac{(k+2)\ell j(j-1)+(i+2)j\ell(\ell-1)}{(i+k+4)(j+\ell-2)} \qquad \text{odd}$$

$$= 0 \qquad\qquad \text{even}$$

$$I20_{ijk\ell} = 2\,\frac{(k+2)(i+2)(i+1)\ell+(i+2)(k+2)(k+1)j}{(i+k+2)(j+\ell)}$$
$$\text{odd}$$

$$= 0 \qquad\qquad \text{even}$$

33

$$M1_{ijkl} = 0 \qquad \text{for } (j+l) \text{ odd}$$

$$= 2\frac{1}{(i+k+3)(j+l+1)} \qquad \text{for } (j+l) \text{ even}$$

$$M2_{ijkl} = M1_{ijkl}$$

$$M3_{ijkl} = I14_{ijkl}$$

$$K1_{ijkl} = I1_{ijkl} + (l/R\gamma)^2(\sin^2\alpha + \frac{(1-\nu)}{2}\cos^2\alpha)I2_{ijkl}$$
$$-(\sin\alpha)(l/R\gamma)I3_{ijkl}$$

$$K2_{ijkl} = (l/R\gamma)(\frac{(1-\nu)}{2}\cos\alpha)I4_{ijkl} + \nu(\cos\alpha)I5_{ijkl}$$
$$-(l/R\gamma)(\sin\alpha)(\cos\alpha)\frac{(1+\nu)}{2}I6_{ijkl})$$

$$K3_{ijkl} = (l/R\gamma)\nu(\cos\alpha)(I7_{ijkl} - (l/R\gamma)(\sin\alpha) \cdot$$
$$I8_{ijkl})$$

$$K4_{ijkl} = \{(1+(h/R)^2/12)(l(\cos\alpha)/R\gamma)^2 + (1+(h/R)^2/3)$$
$$\cdot \frac{(1-\nu)}{2}(l(\sin\alpha)/R\gamma)^2\} I2_{ijkl}$$
$$+ (1+(h/R)^2/3)\frac{(1-\nu)}{2} I1_{ijkl} - (l/R\gamma) \cdot$$
$$(\sin\alpha) I3_{ijkl}$$

$$K5_{1jk\ell} = (\ell(\cos\,\alpha)/R)^2\,I8_{1jk\ell}/\gamma - ((h/R)^2/(12\gamma))\,\cdot$$
$$\{(\ell/R\gamma)^2(1+(1-\nu)\sin^2\alpha)\,I9_{1jk\ell} + \nu\,I10_{1jk\ell}$$
$$- 2(\ell/R\gamma)(\sin\,\alpha)\,I11_{1jk\ell} + 2(1-\nu)\,I12_{1jk\ell}$$
$$- 2(1-\nu)(\ell/R\gamma)(\sin\,\alpha)\,I13_{1jk\ell}\}$$

$$K6_{1jk\ell} = (\ell/R\;)^2\,I14_{1jk\ell}(\cos^2\alpha) + ((h/R)^2/12)\,\cdot$$
$$\{(R/\ell(\cos\,\alpha))^2\,I15_{1jk\ell} + (\ell/R\gamma^2(\cos\,\alpha))^2\,\cdot$$
$$I16_{1jk\ell} + (\tan^2\alpha + \nu)\,I17_{1jk\ell}/\gamma^2$$
$$+ (2(1-\nu)+4\tan^2\alpha)\,I18_{1jk\ell}/\gamma^2 - 2(\ell/R\gamma)\,\cdot$$
$$(\tan\,\alpha)\,I19_{1jk\ell}/\gamma^2(\cos\,\alpha) - 2(\tan\,\alpha)\,\cdot$$
$$(R/\ell\gamma)\,I20_{1jk\ell}/(\cos\,\alpha)\}$$

$$KB_{1jk\ell} = I15_{1jk\ell} + (\ell/b)^4\,I16_{1jk\ell} + (\sin^2\alpha+\nu\cos^2\alpha)\cdot$$
$$(\ell/b)^2\,I17_{1jk\ell} + (2(1-\nu)\cos^2\alpha+4\sin^2\alpha)\,\cdot$$
$$(\ell/b)^2\,I18_{1jk\ell} - 2(\ell/b)^3(\sin\,\alpha)\,I19_{1jk\ell}$$
$$- 2(\ell/b)(\sin\,\alpha)\,I20_{1jk\ell}$$

LIST OF REFERENCES

1. Leissa, A. W., _Vibration of Plates_, NASA SP-160, 1969, N67-62660.

2. Bailey, C. D., "Vibration of Thermally Stressed Plates with Various Boundary Conditions", _AIAA Journal_, Vol. 11, No. 1, January 1973, pp. 14-19.

3. Flax, A. H., "Rayleigh and Ritz Revisited", _AIAA Journal_, Vol. 12, No. 2, February 1974, p. 224.

4. Ritz, W., _Gesommelte Werke_, Societe Soisse de Physique, Paris, 1911.

5. Bailey, C. D., "A New Look at Hamilton's Principle", to appear in _Foundations of Physics_, Issue 2, 1975, Plenum Press, New York – London.

6. Hamilton, W. R., "On a General Method in Dynamics; by which the Study of the Motions of All Free Systems of Attracting or Repelling Points is Reduced to the Search and Differentiation of One Central Relation, or Characteristic Function", Phil. Trans. Roy. Soc., 1834, p. 247.

7. Beres, D. P., "Vibration Analysis of a Completely Free Elliptical Plate", _Journal of Sound and Vibration_, Vol. 34, No. 3, June 8, 1974, pp. 441-443.

8. Miller, M. Z., "Vibration of Thermally Stressed Plates with Point Supports", M.Sc. Thesis, The Ohio State University, March 1972.

9. Goldstein, H., _Classical Mechanics_, Addison-Wesley Pub. Co., Inc., Reading, Mass., 1965.

10. Novozhilov, V. V., _The Theory of Thin Shells_, Noordhoff Limited, Groningen, Netherlands, 1959.

11. Barton, M. V., "Vibration of Rectangular and Skew Cantilever Plates", _J. of Applied Mech._, Vol. 18, No. 1, June 1951, pp. 129-134.

12. Dalley, J. W., and Ripperger, E. A., "Experimental Values of Natural Frequencies for Skew and Rectangular Cantilever Plates", _Proc. Soc. Exp. Stress Anal._, Vol. 9, No.2, 1952, pp. 51-66.

13. Claassen, R. W., "Vibrations of Skew Cantilever Plates", _AIAA Journal_, Vol. 1, No. 5, May 1963, p. 1222.

LIST OF REFERENCES (continued)

14. Craig, R. R., Plass, H. J., and Caughfield, D. A., "Experimental Determination of Frequencies and Mode Shapes of Cantilever and Hub-Pin Plates", Def. Res. Lab. Rept. DRL-518, CR-13, Univ. of Texas, June 1964.

15. Plass, H. J., Gaines, J. H., and Newsom, C. D., "Application of Reissner's Variational Principle to Cantilever Plate Deflection and Vibration Problems", J. of Applied Mech., Vol. 29, No. 1, March 1962, pp. 127-135.

16. Beres, D. P., "A Direct Method for Calculating Flutter Speeds", Proc. of AIAA 10th Annual Meeting and Technical Display, AIAA Paper No. 74-270, Washington, D. C., Jan. 28-30, 1974.

17. Leissa, A. W., Vibration of Shells, NASA SP-288, 1973, N77-186367.

18. Kalnins, A., "Effect of Bending on Vibrations of Spherical Shells", J. of the Acoust. Soc. of Am., Vol. 36, No. 1, January 1964, p. 74.

19. Kraus, H., Thin Elastic Shells, 1967, John Wiley and Sons, Inc., N67-23328.

20. Dreher, J. F., and Leissa, A. W., "Axisymmetric Vibration of thin Conical Shells", Proc. 4th Southwestern Conf. on Theoretical and Applied Mech., (New Orleans, La.), Feb. 29-Mar. 1, 1968, pp. 163-181.

TABLE 1. SKEWED PLATE EIGENVALUES

Mode No.	$\lambda_p = \omega\sqrt{\rho h/D}\ \ell^2\cos^2\alpha$			
	$\alpha = 0°$	$\alpha = 15°$	$\alpha = 30°$	$\alpha = 45°$

$\ell/b = 1.0$; $\nu = 0.3$; AR = 0.5

Mode No.	$\alpha = 0°$	$\alpha = 15°$	$\alpha = 30°$	$\alpha = 45°$
1	3.4948	3.3961	3.0496	2.3547
2	5.3583	5.1684	4.6976	4.1826
3	10.1868	9.7192	8.4568	6.7270
4	19.6377	18.5128	15.4916	11.3675
5	21.8506	21.3351	19.3757	15.6528

$\ell/b = 2.0$; $\nu = 0.3$; AR = 1.0

Mode No.	$\alpha = 0°$	$\alpha = 15°$	$\alpha = 30°$	$\alpha = 45°$
1	3.4746	3.3474	2.9522	2.2688
2	8.5141	8.1242	7.0878	5.6992
3	21.3010	20.7595	19.0494	13.6363
4	27.2027	24.5838	19.4758	16.0858
5	30.9848	31.6375	31.1425	25.7958

$\ell/b = 4.0$; $\nu = 0.3$; AR = 2.0

Mode No.	$\alpha = 0°$	$\alpha = 15°$	$\alpha = 30°$	$\alpha = 45°$
1	3.4468	3.2803	2.7952	2.0489
2	14.8144	14.0529	11.9829	9.0208
3	21.4609	20.8552	18.9474	15.6994
4	48.2295	44.2789	35.4095	25.0949
5	61.7164	61.0880	57.2594	45.9879

$\ell/b = 8.0$; $\nu = 0.3$; AR = 4.0

Mode No.	$\alpha = 0°$	$\alpha = 15°$	$\alpha = 30°$	$\alpha = 45°$
1	3.4214	3.2254	2.6771	1.8925
2	21.3638	19.9221	16.1927	11.2502
3	27.5833	27.0763	25.2054	21.5965
4	61.5278	57.4526	46.9855	33.1829
5	85.2098	83.7205	78.3589	67.5967

TABLE 2.   SKEWED PLATE EIGENVALUES

Mode No.	$\alpha = 30°; \quad \nu = 0.3 ; AR = 1.0$			
	$\lambda_p = \omega\sqrt{\rho h/D}\ \ell^2 \cos^2\alpha$			
	Experiment, Refs. [11], [12]	Direct Solution, Beres	Beam Functions, Claassen [13]	Experiment, Ref. [14]
1	2.87	2.9522	2.96	2.97
2	6.92	7.0878	7.24	6.95
3	18.38	19.0494	19.1	18.57
4	19.15	19.4758	19.6	19.82
5	30.48	31.1425	31.8	————

TABLE 3. SKEWED PLATE EIGENVALUES

Mode No.	$\alpha = 45°$; $\nu = 0.3$; AR $= 1.0$ $\lambda_p = \omega\sqrt{\rho h/D} \; \ell^2 \cos^2\alpha$			
	Experiment, Refs. [11], [12]	Direct Solution, Beres	Reissner's Theorem, Ref. [15]	Experiment, Ref. [14]
1	2.13	2.2688	2.06	2.31
2	5.53	5.6992	5.63	5.48
3	13.26	13.6363	13.86	13.31
4	15.06	16.0858	————	15.90
5	25.09	25.7958	————	————

TABLE 4. HELICOIDAL SHELL EIGENVALUES

$$\ell/R = 0.2 \qquad h/R = 0.01 \qquad \nu = 0.3 \qquad \gamma = 0.1 \text{ rad}$$

α = 0°

Mode No.	$\lambda_s = \omega \cdot \sqrt{\rho(1-\nu^2)/E}\,\ell\cos\alpha$	% of strain energy due to membrane	% of strain energy due to bending	generalized mass
1	0.055033	16.99	83.01	9.1242
2	0.12315	0.40	99.60	1.6942
3	0.31920	6.17	93.83	9.0570
4	0.39806	0.79	99.21	6.5230
5	0.45040	0.63	99.37	3.0463

α = 15°

Mode No.	$\lambda_s = \omega \cdot \sqrt{\rho(1-\nu^2)/E}\,\ell\cos\alpha$	% of strain energy due to membrane	% of strain energy due to bending	generalized mass
1	0.054025	14.07	85.93	1.3454
2	0.12266	2.06	97.94	1.2093
3	0.32124	5.35	94.65	2.9140
4	0.37089	0.45	99.55	1.1622
5	0.48135	1.26	98.74	8.9363

α = 30°

Mode No.	$\lambda_s = \omega \cdot \sqrt{\rho(1-\nu^2)/E}\,\ell\cos\alpha$	% of strain energy due to membrane	% of strain energy due to bending	generalized mass
1	0.051386	7.86	92.14	5.4171
2	0.12108	4.62	95.38	6.7129
3	0.32675	2.29	97.71	4.6053
4	0.33108	1.63	98.37	4.5698
5	0.53356	10.22	89.78	1.5491

α = 45°

Mode No.	$\lambda_s = \omega \cdot \sqrt{\rho(1-\nu^2)/E}\,\ell\cos\alpha$	% of strain energy due to membrane	% of strain energy due to bending	generalized mass
1	0.046954	2.50	97.50	1.1615
2	0.11846	4.64	95.36	1.1419
3	0.28031	0.91	99.09	7.0787
4	0.33110	1.81	98.19	1.4521
5	0.45252	98.27	1.73	4.0290

441

TABLE 5. HELICOIDAL SHELL EIGENVALUES

$\ell/R = 0.8 \qquad h/R = 0.01 \qquad \nu = 0.3 \qquad \gamma = 0.1$ rad

$\alpha = 0°$

Mode No.	$\lambda_S = \omega \cdot$ $\sqrt{\rho(1-\nu^2)/E}\,\ell\cos\alpha$	% of strain energy due to membrane	% of strain energy due to bending	generalized mass
1	0.013817	20.41	79.59	6.4158
2	0.085751	19.30	80.70	2.1607
3	0.099644	0.33	99.67	3.9252
4	0.23240	99.91	0.09	5.9594
5	0.24289	16.69	83.31	2.6617

$\alpha = 15°$

Mode No.	$\lambda_S = \omega \cdot$ $\sqrt{\rho(1-\nu^2)/E}\,\ell\cos\alpha$	% of strain energy due to membrane	% of strain energy due to bending	generalized mass
1	0.013123	15.63	84.37	1.0263
2	0.078118	13.04	86.96	3.3733
3	0.10304	5.78	94.22	2.2918
4	0.21436	49.33	50.67	3.7436
5	0.23223	60.25	39.75	1.2606

$\alpha = 30°$

Mode No.	$\lambda_S = \omega \cdot$ $\sqrt{\rho(1-\nu^2)/E}\,\ell\cos\alpha$	% of strain energy due to membrane	% of strain energy due to bending	generalized mass
1	0.011659	7.73	92.27	1.9527
2	0.064690	9.42	90.58	2.8079
3	0.10389	10.48	89.52	6.6308
4	0.18166	46.00	54.00	2.4239
5	0.22456	46.95	53.05	8.2090

$\alpha = 45°$

Mode No.	$\lambda_S = \omega \cdot$ $\sqrt{\rho(1-\nu^2)/E}\,\ell\cos\alpha$	% of strain energy due to membrane	% of strain energy due to bending	generalized mass
1	0.009890	3.54	96.46	4.7196
2	0.050025	10.84	89.16	3.7014
3	0.087251	17.06	82.94	1.2557
4	0.15069	28.53	71.47	2.9546
5	0.20298	41.29	58.71	3.1705

TABLE 6. HELICOIDAL SHELL EIGENVALUES

$$l/R = 0.8 \qquad h/R = 0.01 \qquad \nu = 0.3 \qquad \alpha = 0°$$

$\gamma = 0.1$ rad

Mode No.	$\lambda_s = \omega \cdot \sqrt{\rho(1-\nu^2)/E} \cdot l/\cos\alpha$	% of strain energy due to membrane	% of strain energy due to bending	generalized mass
1	0.013817	20.41	79.59	6.4158
2	0.085751	19.30	80.70	2.1607
3	0.099644	0.33	99.67	3.9252
4	0.23240	99.91	0.09	5.9594
5	0.24289	16.69	83.31	2.6617

$\gamma = 0.3$ rad

Mode No.	$\lambda_s = \omega \cdot \sqrt{\rho(1-\nu^2)/E} \cdot l/\cos\alpha$	% of strain energy due to membrane	% of strain energy due to bending	generalized mass
1	0.042681	18.11	81.89	2.1815
2	0.052883	89.74	10.26	1.3872
3	0.15929	30.59	69.41	3.6941
4	0.15974	8.51	91.49	1.5465
5	0.20723	38.07	61.93	3.7834

$\gamma = 0.5$ rad

Mode No.	$\lambda_s = \omega \cdot \sqrt{\rho(1-\nu^2)/E} \cdot l/\cos\alpha$	% of strain energy due to membrane	% of strain energy due to bending	generalized mass
1	0.049641	69.01	30.99	2.6410
2	0.061378	18.17	81.83	1.3951
3	0.14914	89.96	10.04	1.5511
4	0.17898	33.19	66.81	9.4340
5	0.17959	39.35	60.65	9.5614

$\gamma = 0.7$ rad

Mode No.	$\lambda_s = \omega \cdot \sqrt{\rho(1-\nu^2)/E} \cdot l/\cos\alpha$	% of strain energy due to membrane	% of strain energy due to bending	generalized mass
1	0.053481	48.87	51.13	2.1032
2	0.066911	56.84	43.16	6.3277
3	0.13920	53.49	46.51	1.7002
4	0.18983	36.29	63.71	2.8389
5	0.20016	61.72	38.28	1.6372

TABLE 7. HELICOIDAL SHELL EIGENVALUES

$$\ell/R = 0.8 \qquad h/R = 0.01 \qquad \nu = 0.3 \qquad \alpha = 30°$$

$\gamma = 0.1$ rad

Mode No.	$\lambda_s = \omega \cdot \sqrt{\rho(1-\nu^2)/E}\, \ell\cos\alpha$	% of strain energy due to membrane	% of strain energy due to bending	generalized mass
1	0.011659	7.73	92.27	1.9527
2	0.064690	9.42	90.58	2.8079
3	0.10389	10.48	89.52	6.6308
4	0.18166	46.00	54.00	2.4239
5	0.22456	46.95	53.05	8.2090

$\gamma = 0.3$ rad

Mode No.	$\lambda_s = \omega \cdot \sqrt{\rho(1-\nu^2)/E}\, \ell\cos\alpha$	% of strain energy due to membrane	% of strain energy due to bending	generalized mass
1	0.019676	21.59	78.41	1.0371
2	0.069371	50.44	49.56	1.7562
3	0.12406	31.37	68.63	1.7545
4	0.15527	28.02	71.98	3.8605
5	0.24472	31.03	68.97	3.8958

$\gamma = 0.5$ rad

Mode No.	$\lambda_s = \omega \cdot \sqrt{\rho(1-\nu^2)/E}\, \ell\cos\alpha$	% of strain energy due to membrane	% of strain energy due to bending	generalized mass
1	0.023129	23.54	76.46	1.6050
2	0.082180	42.44	57.56	3.5571
3	0.13052	32.89	67.11	6.0257
4	0.14811	83.05	16.95	2.5619
5	0.16823	39.59	60.41	2.2914

$\gamma = 0.7$ rad

Mode No.	$\lambda_s = \omega \cdot \sqrt{\rho(1-\nu^2)/E}\, \ell\cos\alpha$	% of strain energy due to membrane	% of strain energy due to bending	generalized mass
1	0.025434	32.31	67.69	1.1878
2	0.094740	47.98	52.02	7.1253
3	0.13482	68.49	31.51	1.6844
4	0.14516	44.22	55.78	1.6861
5	0.20398	66.83	33.17	1.6626

TABLE 8. HELICOIDAL SHELL EIGENVALUES

$h/R = 0.01$ $\nu = 0.3$ $\alpha = 0°$ $\gamma = 0.1$ rad

$l/R = 0.1$

Mode No.	$\lambda_s = \omega \cdot \sqrt{\rho(1-\nu^2)/E'} \, l \cos\alpha$	% of strain energy due to membrane	% of strain energy due to bending	generalized mass
1	0.10619	9.75	90.25	1.1958
2	0.15516	0.67	99.33	1.0221
3	0.29847	0.49	99.51	8.8834
4	0.56742	0.15	99.85	3.5975
5	0.63881	1.19	98.81	1.6759

$l/R = 0.2$

Mode No.	$\lambda_s = \omega \cdot \sqrt{\rho(1-\nu^2)/E'} \, l \cos\alpha$	% of strain energy due to membrane	% of strain energy due to bending	generalized mass
1	0.055033	16.99	83.01	9.1242
2	0.12315	0.40	99.60	1.6942
3	0.31920	6.17	93.83	9.0570
4	0.39806	0.79	99.21	6.5230
5	0.45040	0.63	99.37	3.0463

$l/R = 0.4$

Mode No.	$\lambda_s = \omega \cdot \sqrt{\rho(1-\nu^2)/E'} \, l \cos\alpha$	% of strain energy due to membrane	% of strain energy due to bending	generalized mass
1	0.02769	19.53	80.47	2.1162
2	0.10712	0.29	99.71	1.6425
3	0.16787	15.08	84.92	2.3493
4	0.35020	0.49	99.51	2.7004
5	0.41555	99.97	0.03	2.2949

$l/R = 0.8$

Mode No.	$\lambda_s = \omega \cdot \sqrt{\rho(1-\nu^2)/E'} \, l \cos\alpha$	% of strain energy due to membrane	% of strain energy due to bending	generalized mass
1	0.013817	20.41	79.59	6.4158
2	0.085751	19.30	80.70	2.1607
3	0.099644	0.33	99.67	3.9252
4	0.23240	99.91	0.09	5.9594
5	0.24289	16.69	83.31	2.6617

TABLE 9. HELICOIDAL SHELL EIGENVALUES

$h/R = 0.01$ $\nu = 0.3$ $\alpha = 30°$ $\gamma = 0.1$ rad

$\ell/R = 0.1$

Mode No.	$\lambda_S = \omega \cdot \sqrt{\rho(1-\nu^2)/E}\,\ell\cos\alpha$	% of strain energy due to membrane	% of strain energy due to bending	generalized mass
1	0.10377	3.80	96.20	1.3865
2	0.15990	4.03	95.97	9.5907
3	0.28535	0.40	99.60	2.4998
4	0.52231	0.16	99.84	1.5343
5	0.65908	1.07	98.93	2.0466

$\ell/R = 0.2$

Mode No.	$\lambda_S = \omega \cdot \sqrt{\rho(1-\nu^2)/E}\,\ell\cos\alpha$	% of strain energy due to membrane	% of strain energy due to bending	generalized mass
1	0.051386	7.86	92.14	5.4171
2	0.12108	4.62	95.38	6.7129
3	0.32675	2.29	97.71	4.6053
4	0.33108	1.63	98.37	4.5698
5	0.53356	10.22	89.78	1.5491

$\ell/R = 0.4$

Mode No.	$\lambda_S = \omega \cdot \sqrt{\rho(1-\nu^2)/E}\,\ell\cos\alpha$	% of strain energy due to membrane	% of strain energy due to bending	generalized mass
1	0.024325	7.86	92.14	1.5070
2	0.10082	5.09	94.91	4.6684
3	0.16408	7.83	92.17	1.5731
4	0.29471	9.75	90.25	3.8707
5	0.35614	92.90	7.80	3.2429

$\ell/R = 0.8$

Mode No.	$\lambda_S = \omega \cdot \sqrt{\rho(1-\nu^2)/E}\,\ell\cos\alpha$	% of strain energy due to membrane	% of strain energy due to bending	generalized mass
1	0.011659	7.73	92.27	1.9527
2	0.064690	9.42	90.58	2.8079
3	0.10389	10.48	89.52	6.6308
4	0.18166	46.00	54.00	2.4239
5	0.22456	46.95	53.05	8.2090

Figure 1. Helicoidal Shell
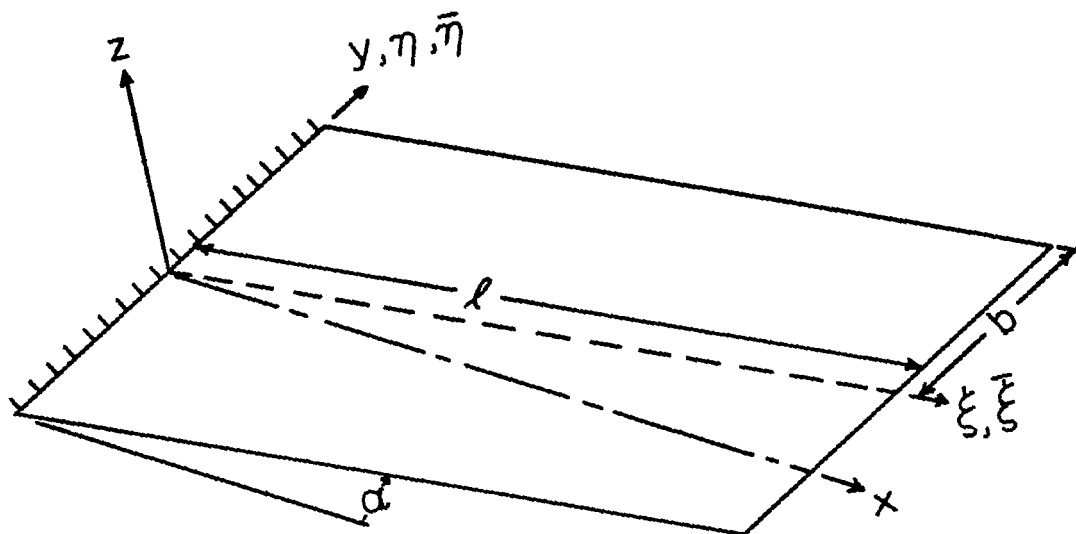
Figure 2. SKEWED PLATE
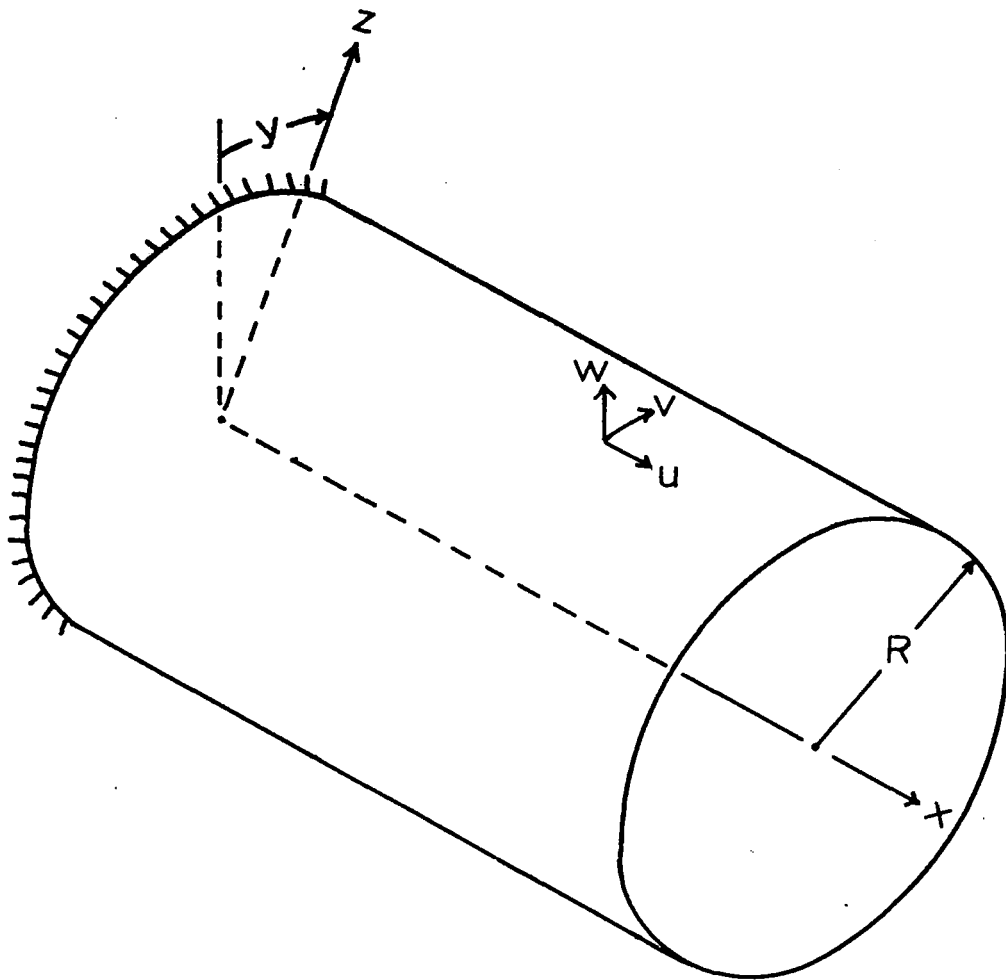
FIGURE 3. RIGHT CIRCULAR
CYLINDER WITH
COORDINATE SYSTEM
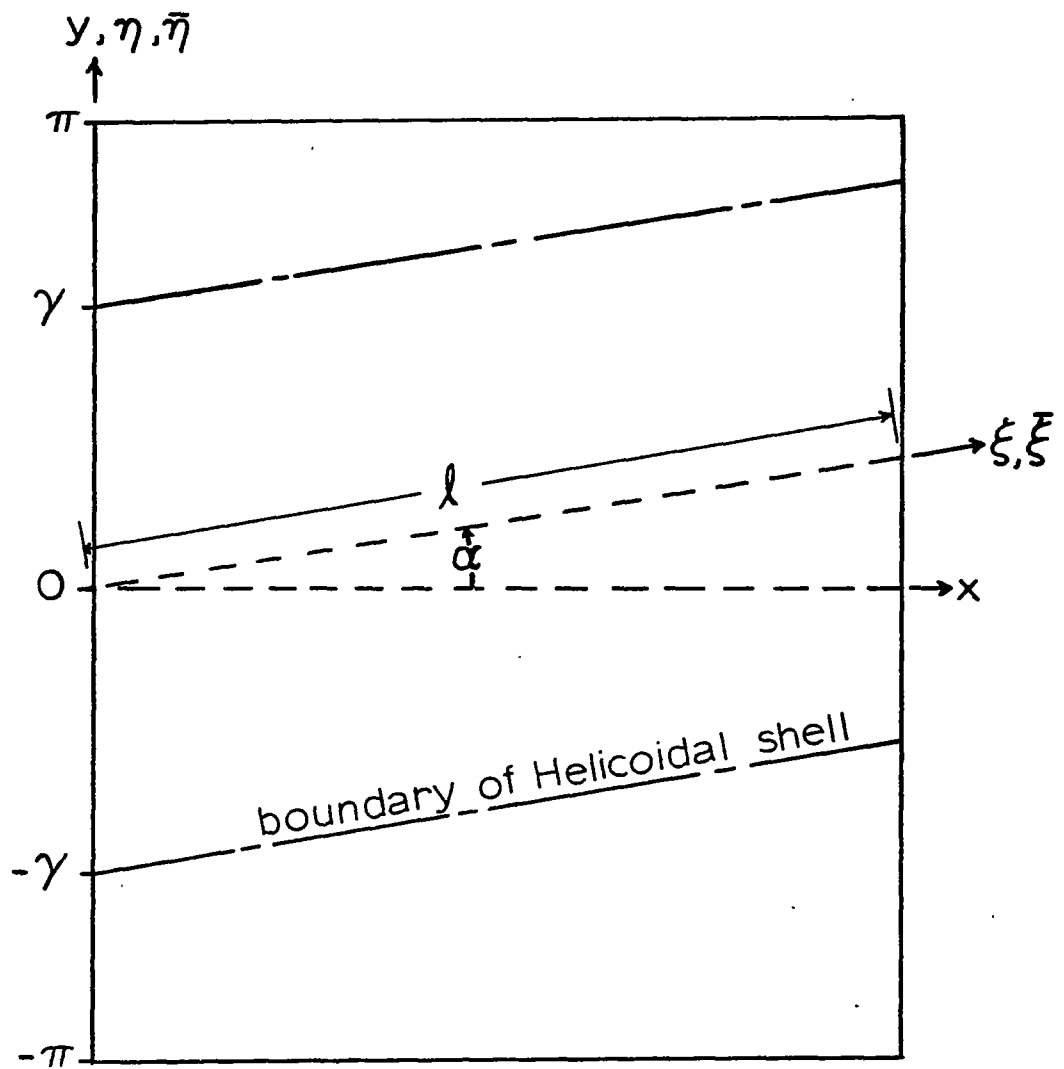
FIGURE 4. RIGHT CIRCULAR
CYLINDER CUT ALONG $y = \pi$
AND DEVELOPED INTO THE
PLANE, SHOWING THE HELI-
COIDAL SHELL AND SKEWED
COORDINATE SYSTEM
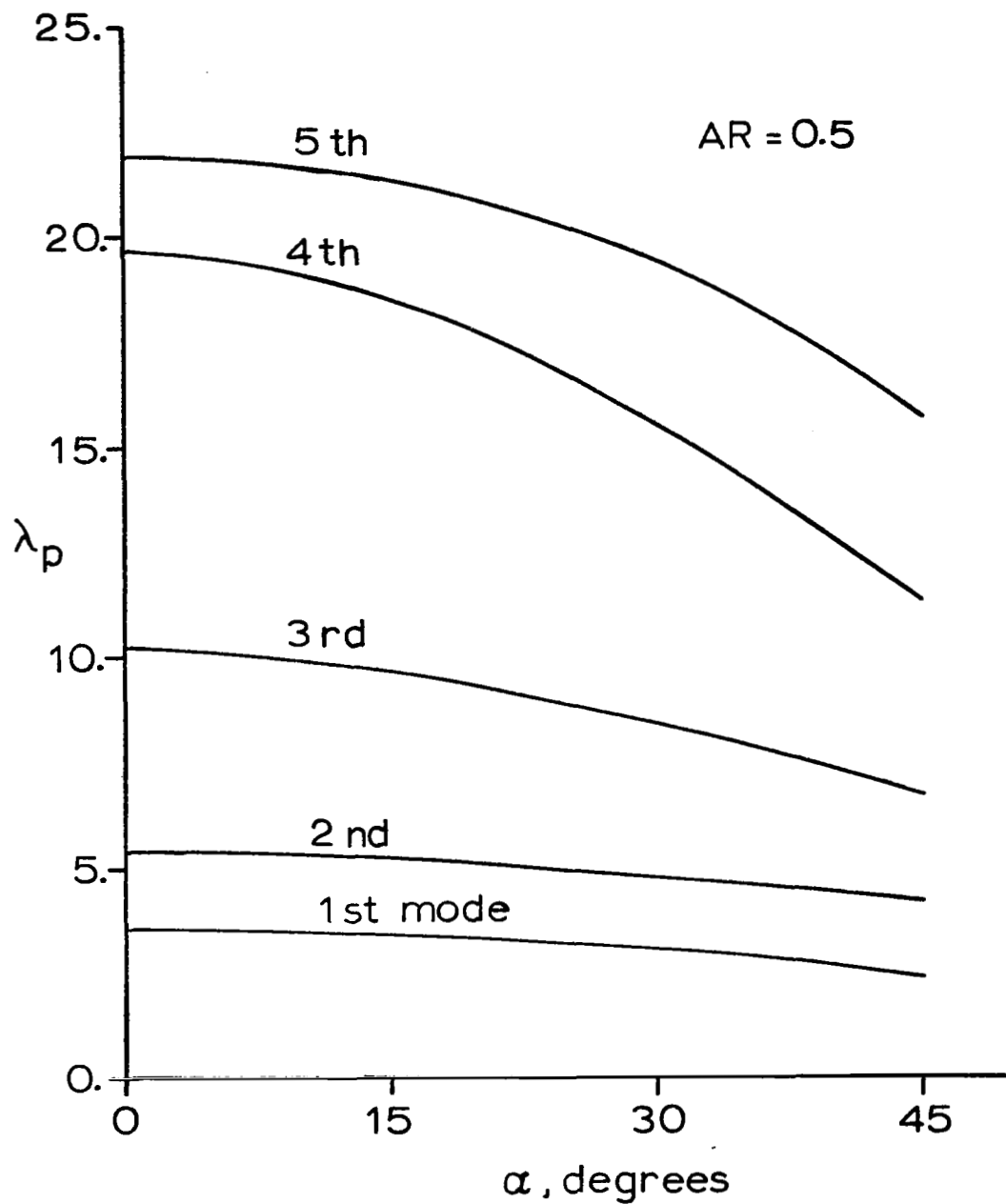
FIGURE 5. SKEWED PLATE
EIGENVALUES vs α, AR=0.5
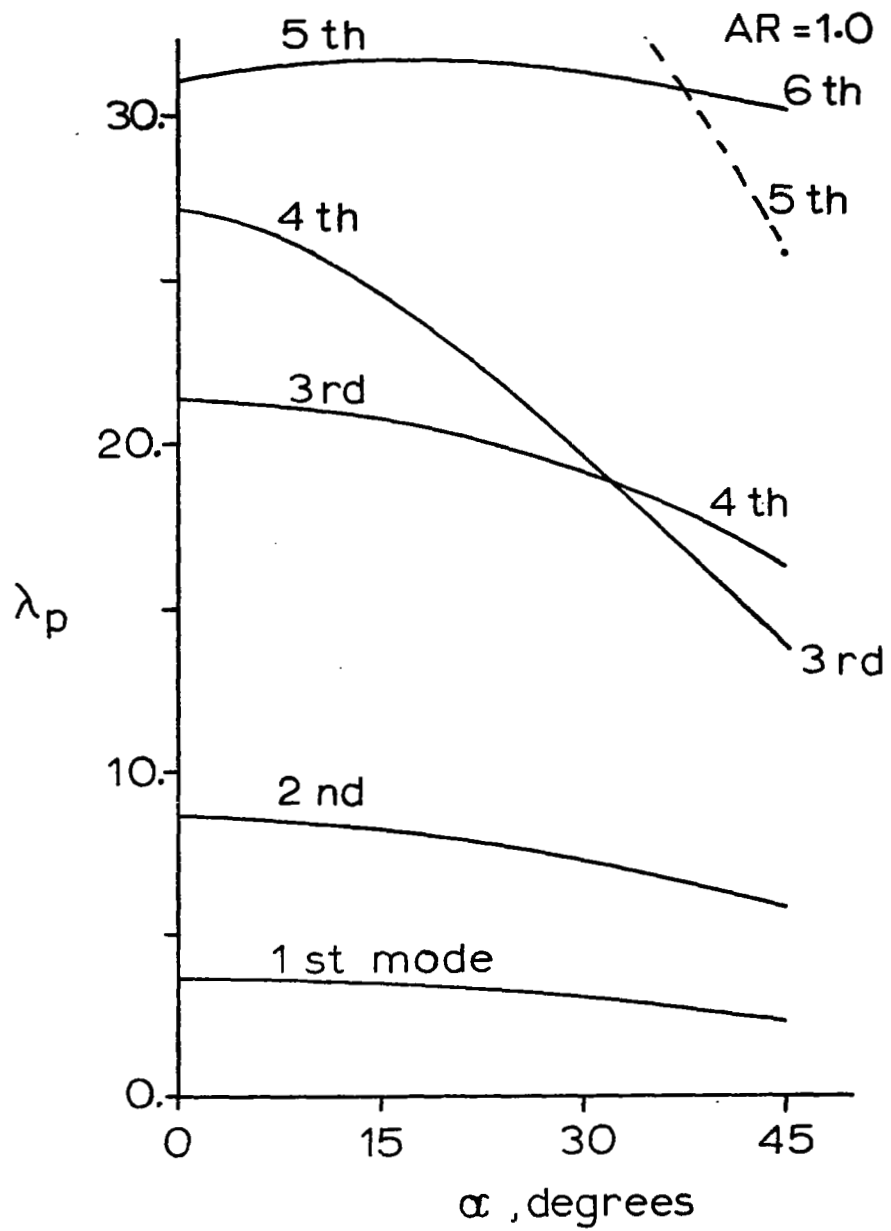
FIGURE 6. SKEWED PLATE
EIGENVALUES vs α, AR=1.0
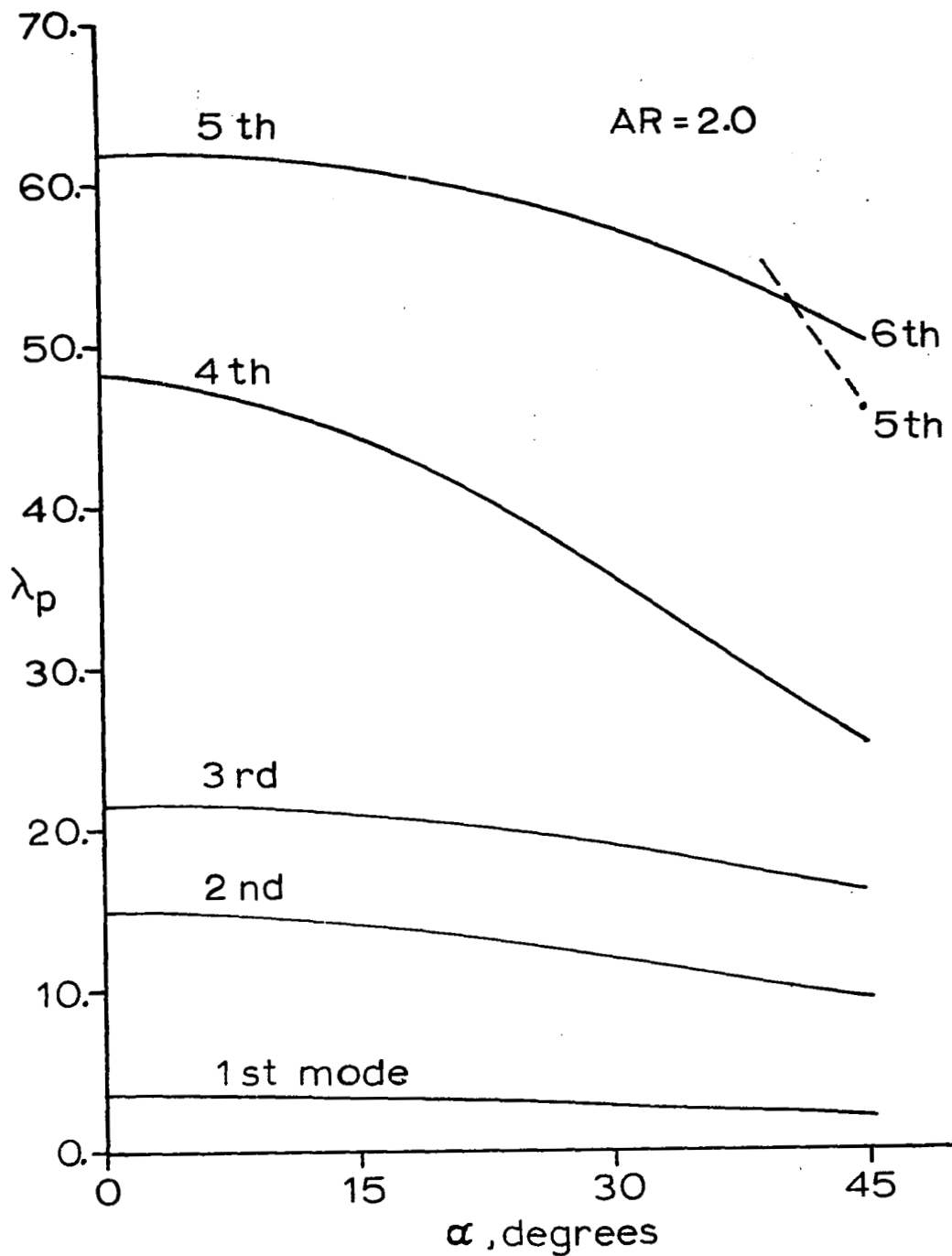
FIGURE 7. SKEWED PLATE
EIGENVALUES vs α , AR = 2.0

53
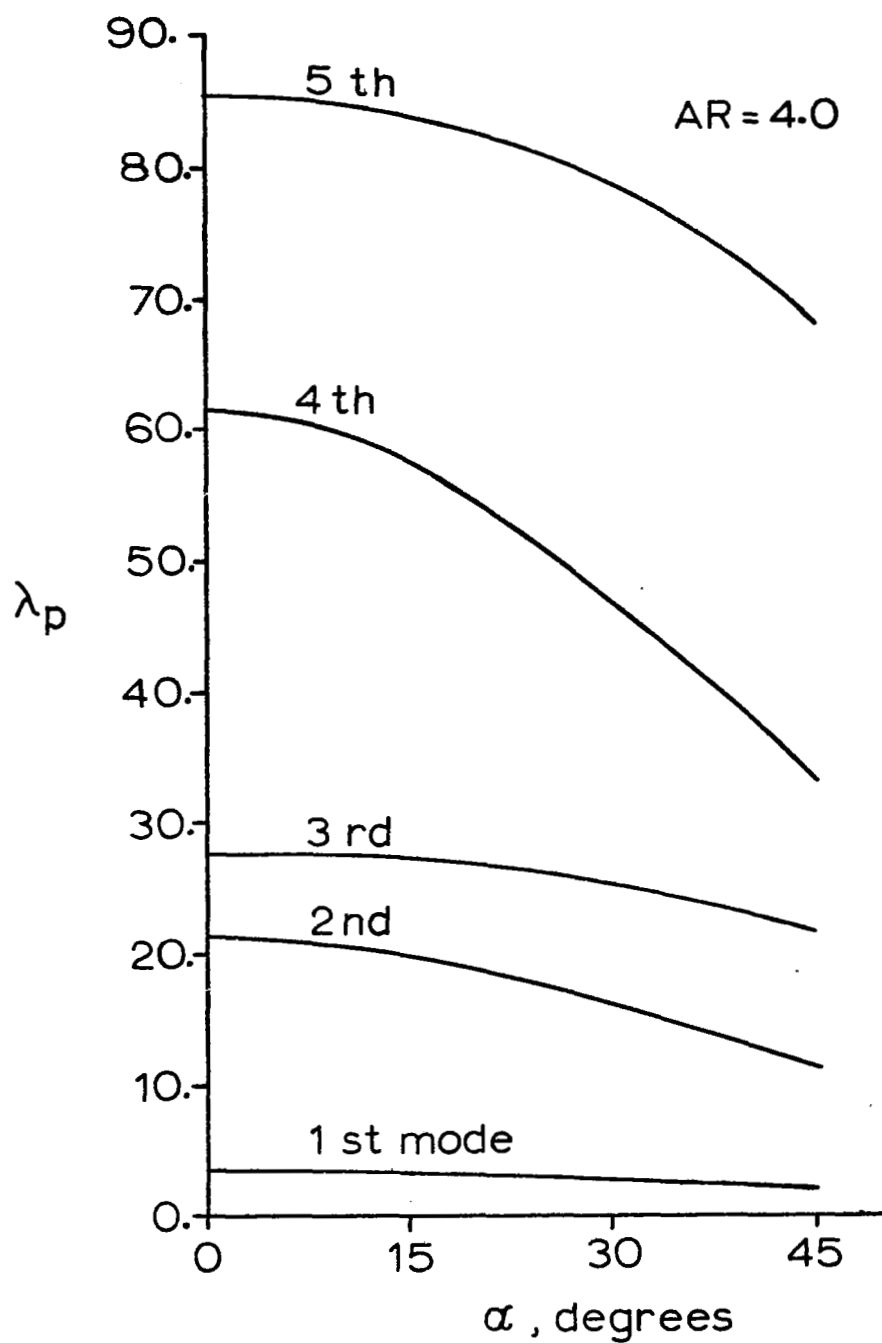
FIGURE 8. SKEWED PLATE
EIGENVALUES vs α, AR = 4.0
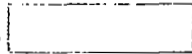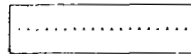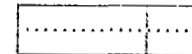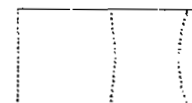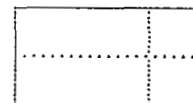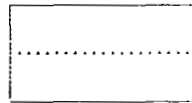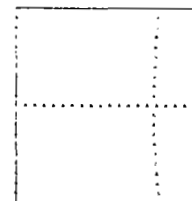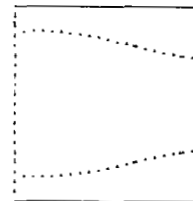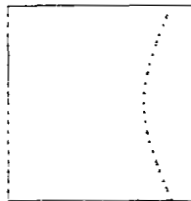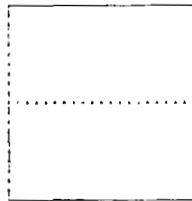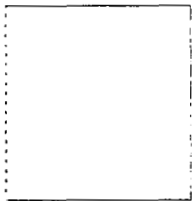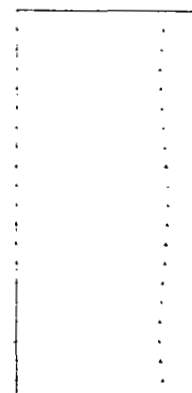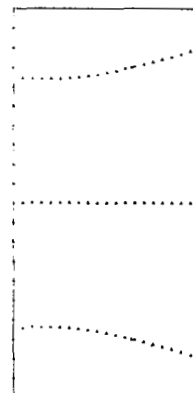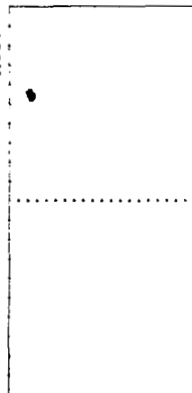
Figure 9. SKEWED PLATE , w NODAL PATTERNS

$\alpha = 15°$

Mode No. →

AR
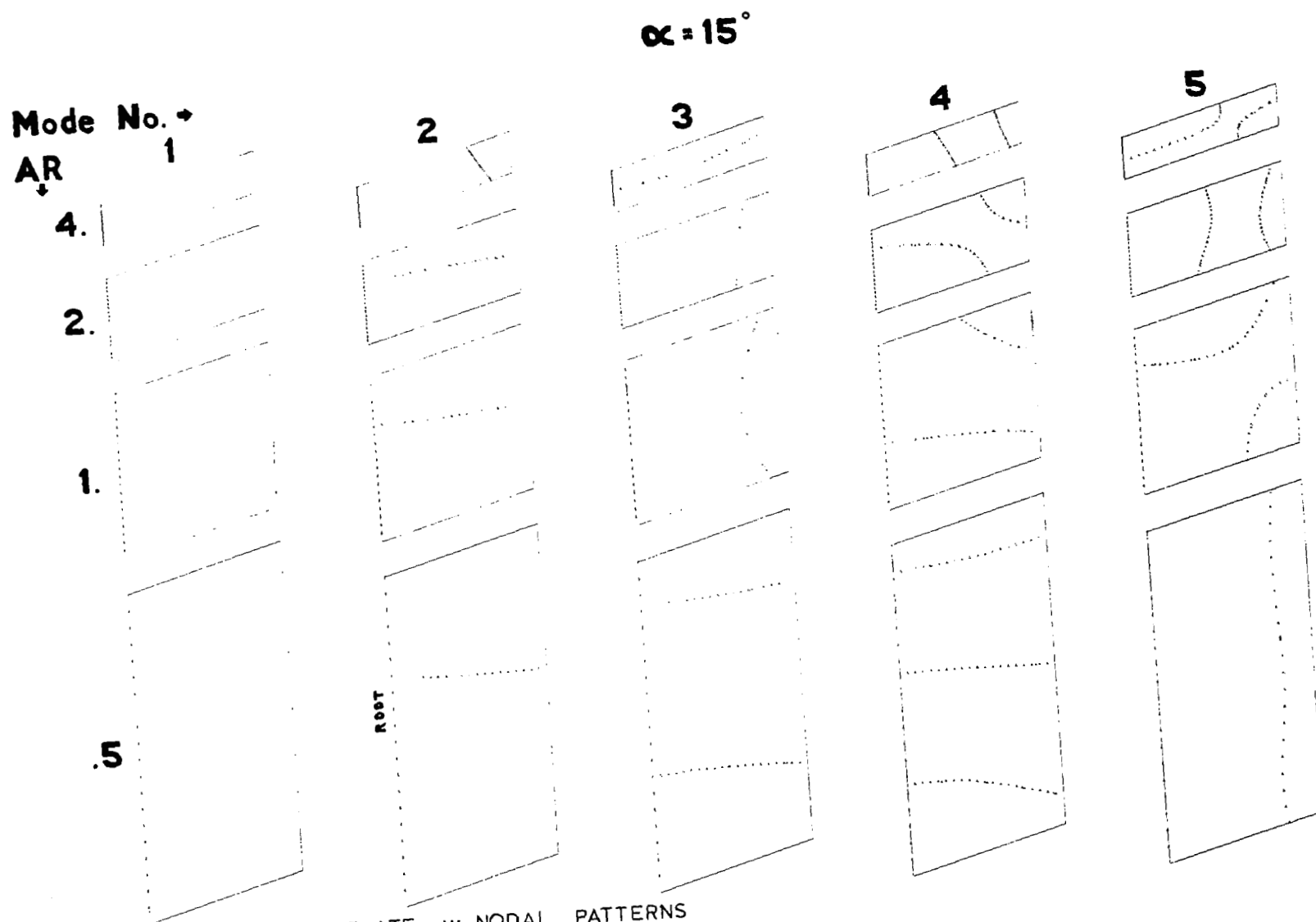
Figure 10. SKEWED PLATE , w NODAL PATTERNS

56

$\alpha = 30°$

Mode No. →

AR ↓

1 2 3 4 5

4.

2.

1.

.5

ROOT
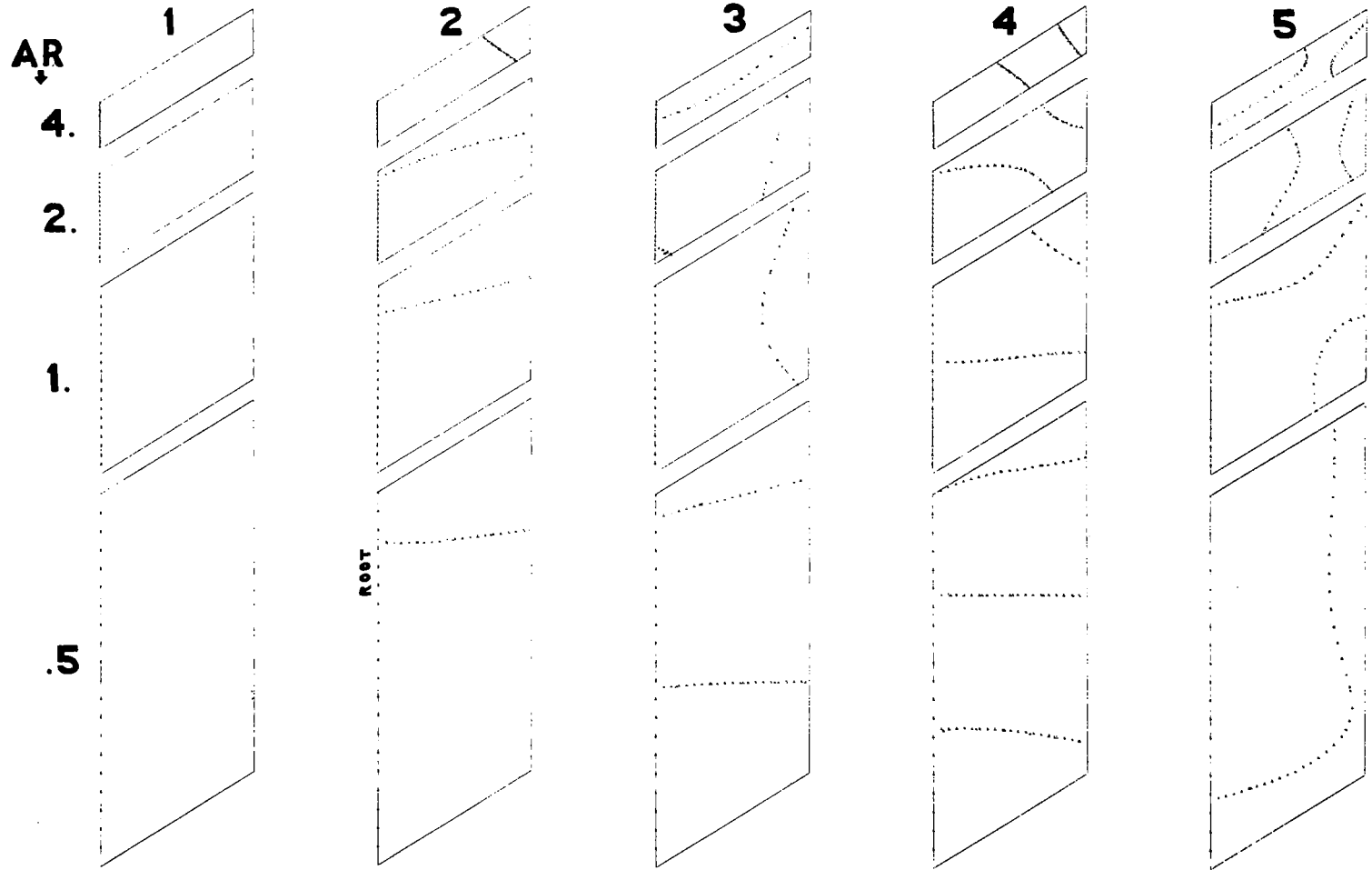
Figure 11.   SKEWED   PLATE , w NODAL PATTERNS

Mode No. ●   **∝ = 45°**

1   **2**   **3**   **4**   **5**

AR
↓
4.

2.

1.

.5

ROOT
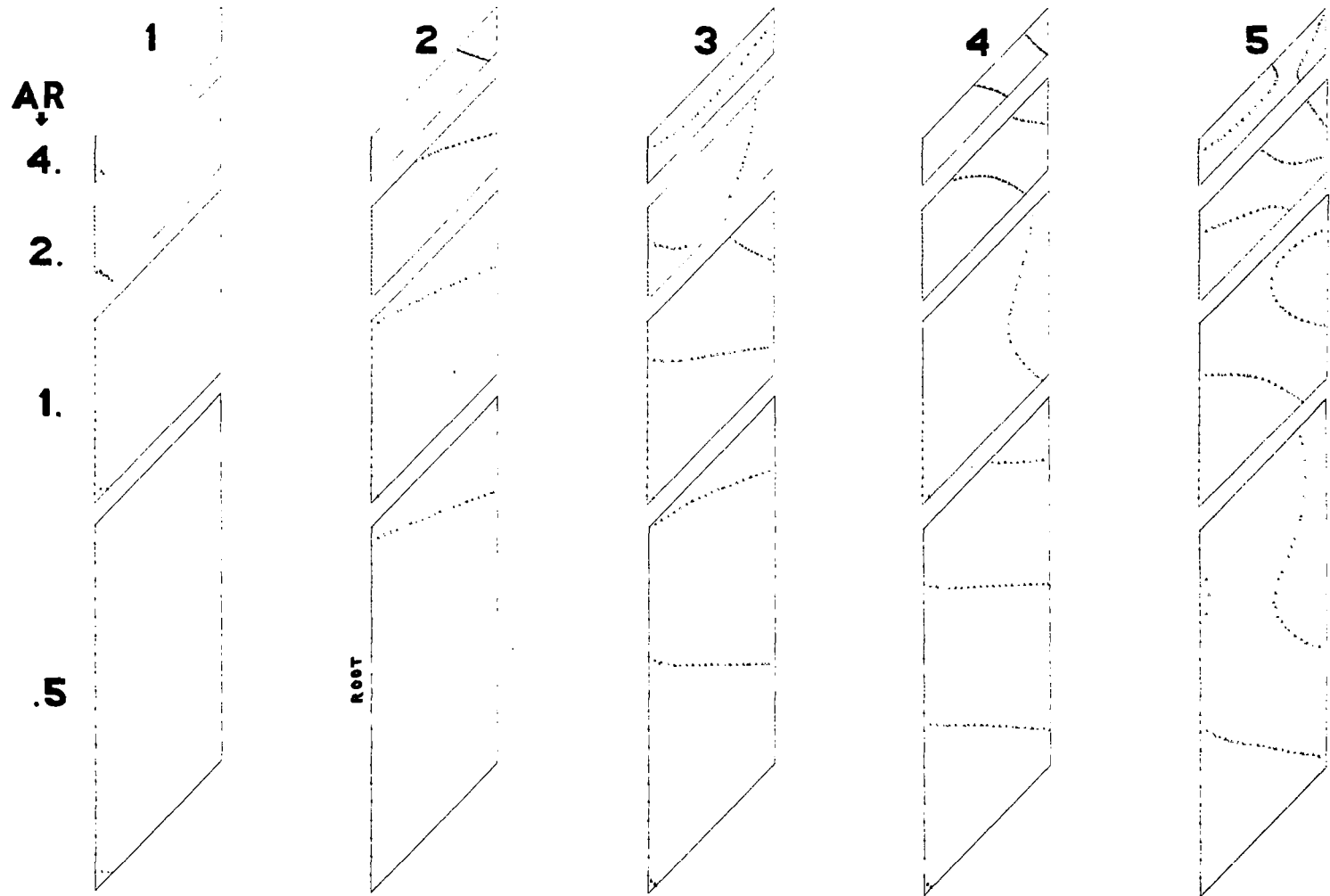
Figure 12. SKEWED PLATE , w NODAL PATTERNS
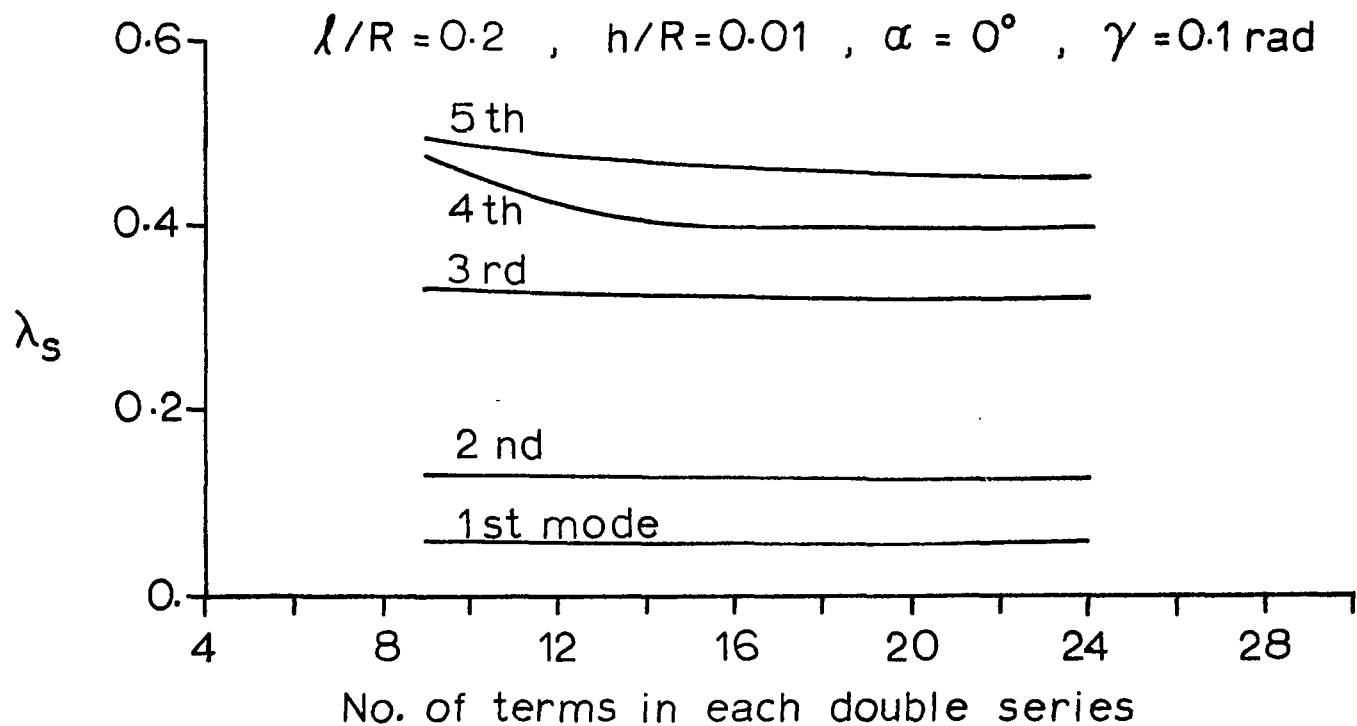
FIGURE 13. CONVERGENCE OF EIGENVALUES
FOR HELICOIDAL SHELL

$l/R = 0.2$, $h/R = 0.01$, $\alpha = 45°$, $\gamma = 0.1$ rad

5 th

4 th

3 rd

2 nd

1 st mode

λ_s

No. of terms in each double series
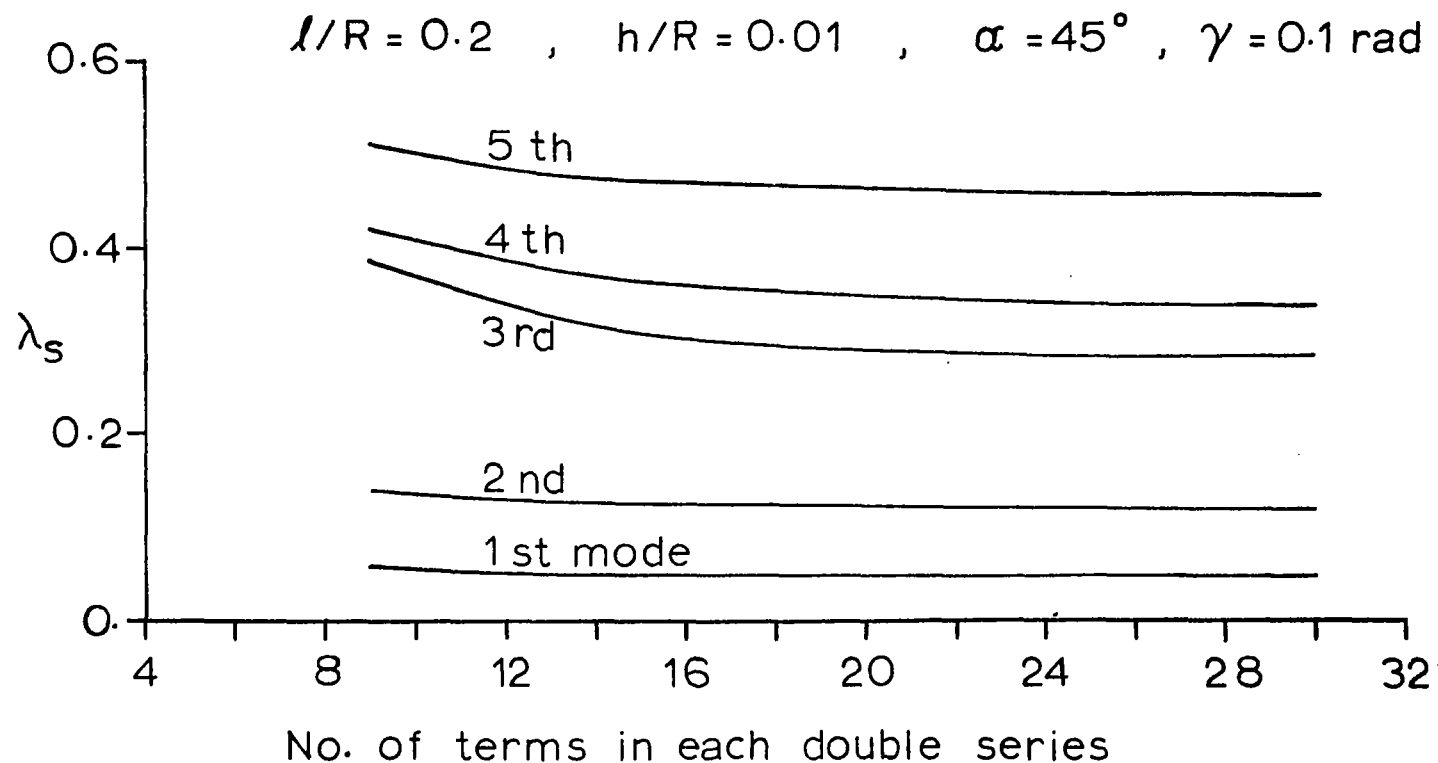
FIGURE 14. CONVERGENCE OF EIGENVALUES
FOR HELICOIDAL SHELL

$l/R = 0.8$, $h/R = 0.01$, $\alpha = 15°$, $\gamma = 0.1\,$rad

5 th

4 th

3 rd

2 nd

1 st mode

λ_s

No. of terms in each double series
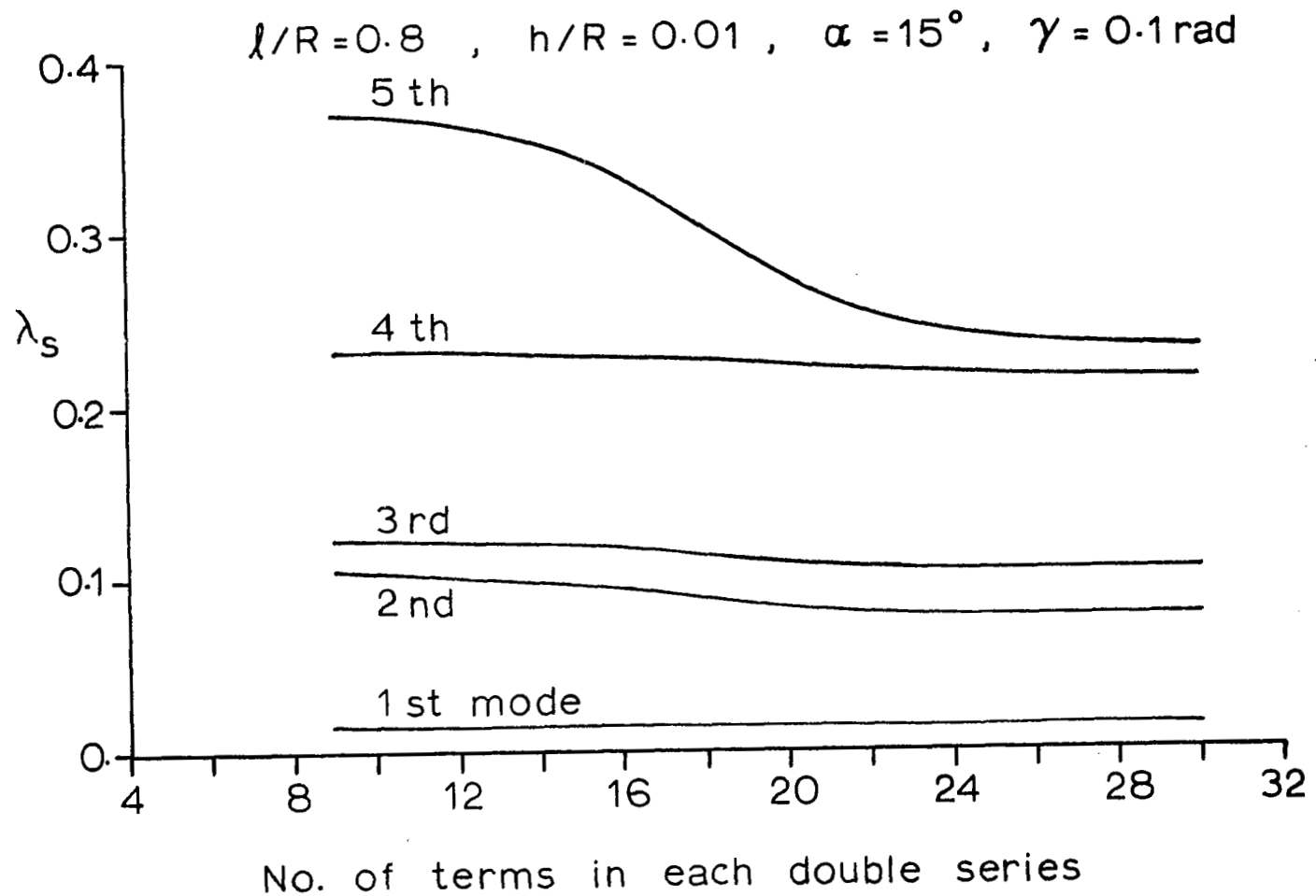
FIGURE 15. CONVERGENCE OF EIGENVALUES
FOR HELICOIDAL SHELL
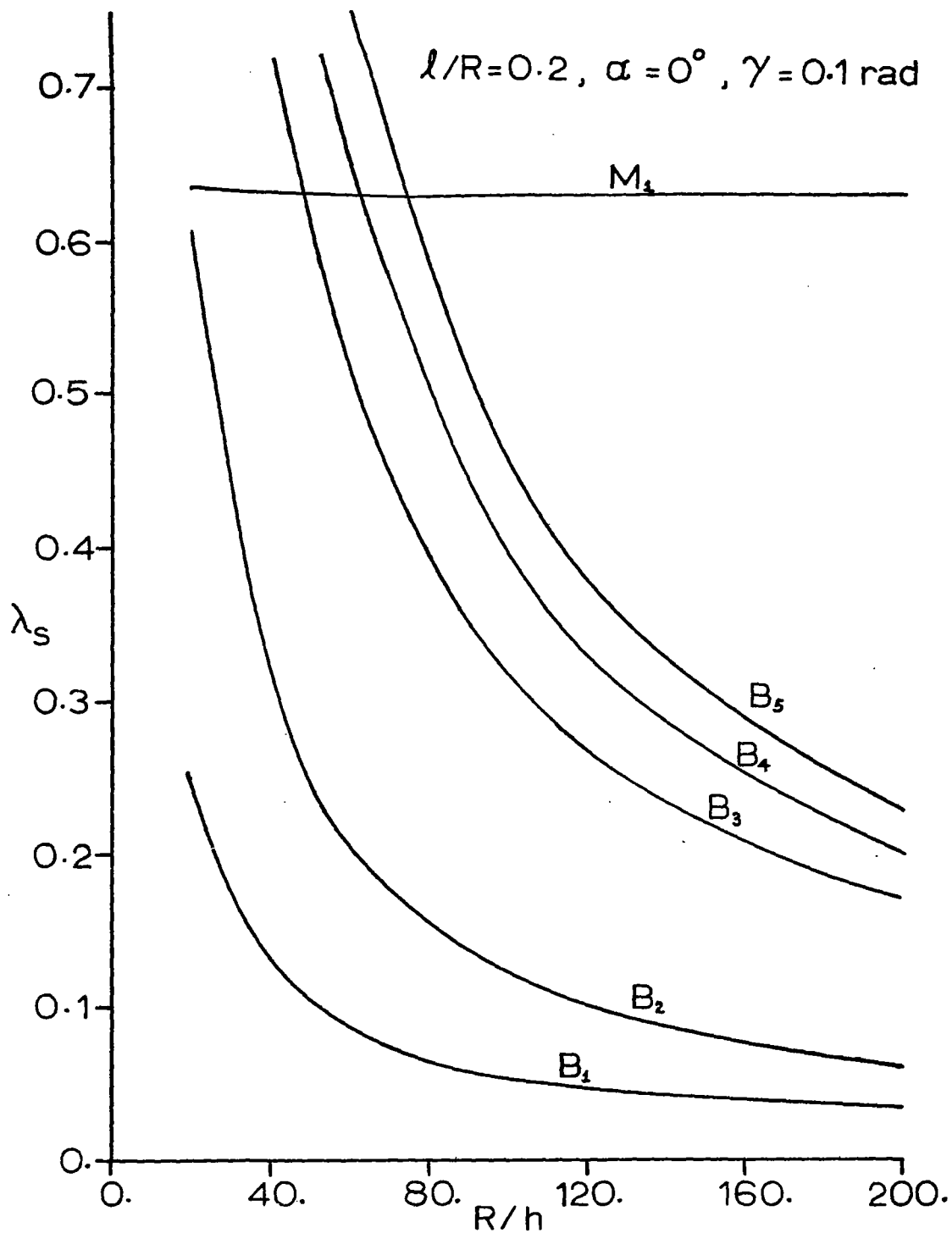
FIGURE 16. HELICOIDAL SHELL
EIGENVALUES vs R/h
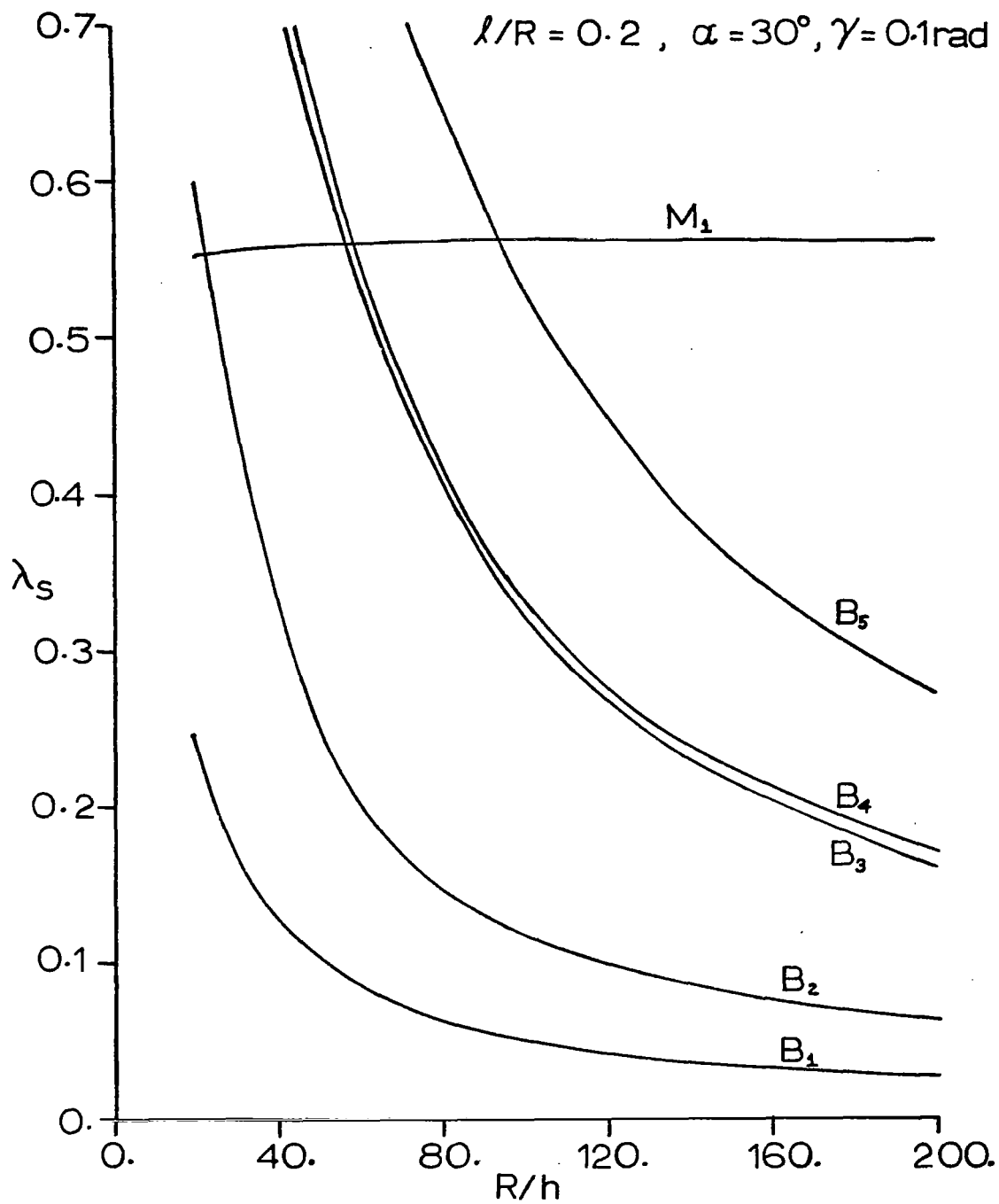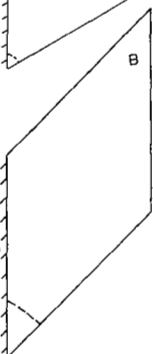
FIGURE 17. HELICOIDAL SHELL
EIGENVALUES vs R/h
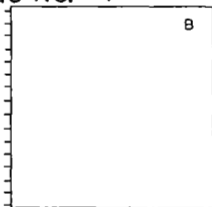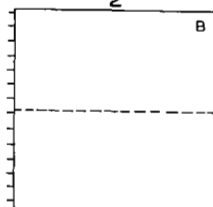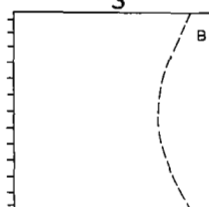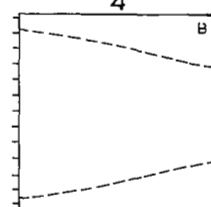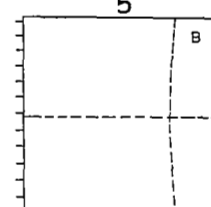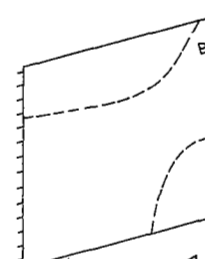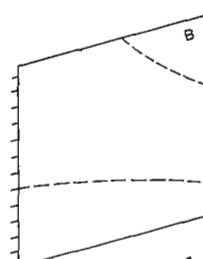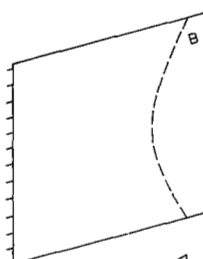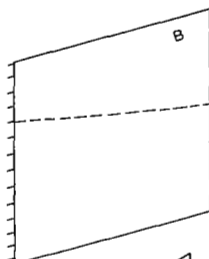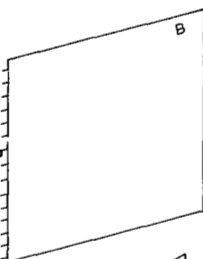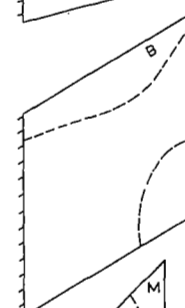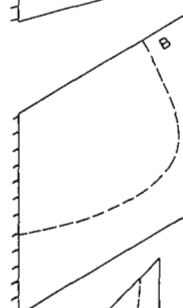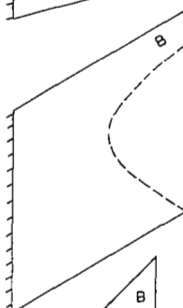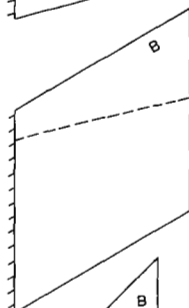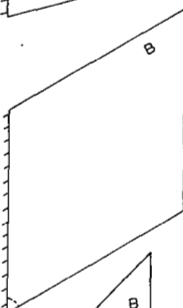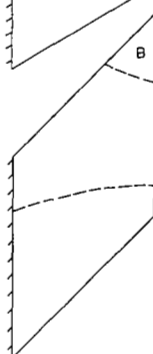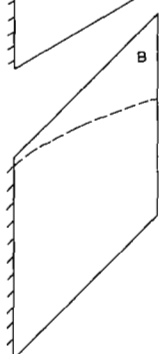
Figure 18. HELICOIDAL SHELL , w NODAL PATTERNS , $\ell/R = 0.2$, $h/R = 0.01$, $\gamma = 0.1$ rad
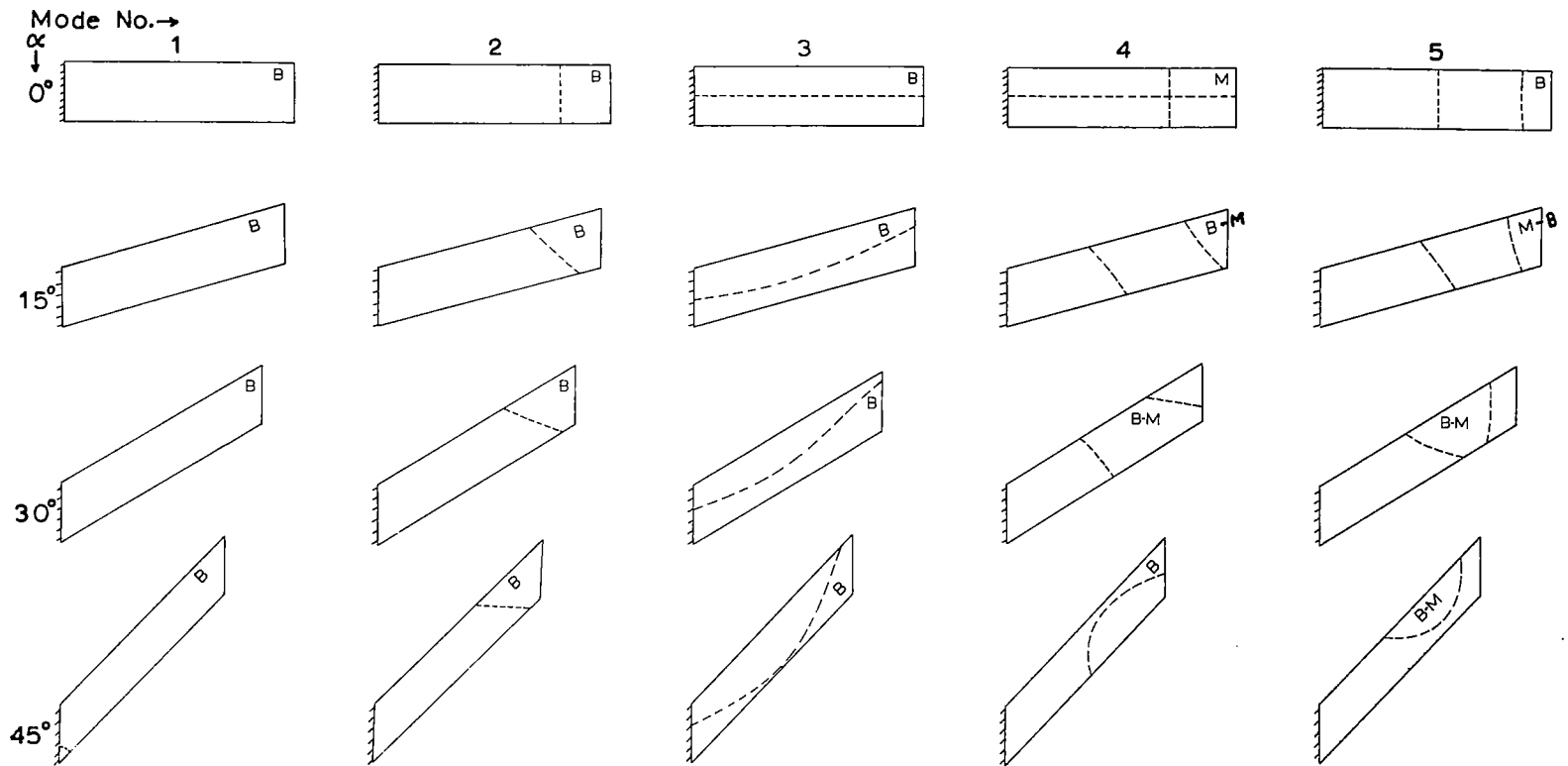
Figure 19. HELICOIDAL SHELL , w NODAL PATTERNS , $\ell/R = 0.8$, $h/R = 0.01$, $\gamma = 0.1$ rad

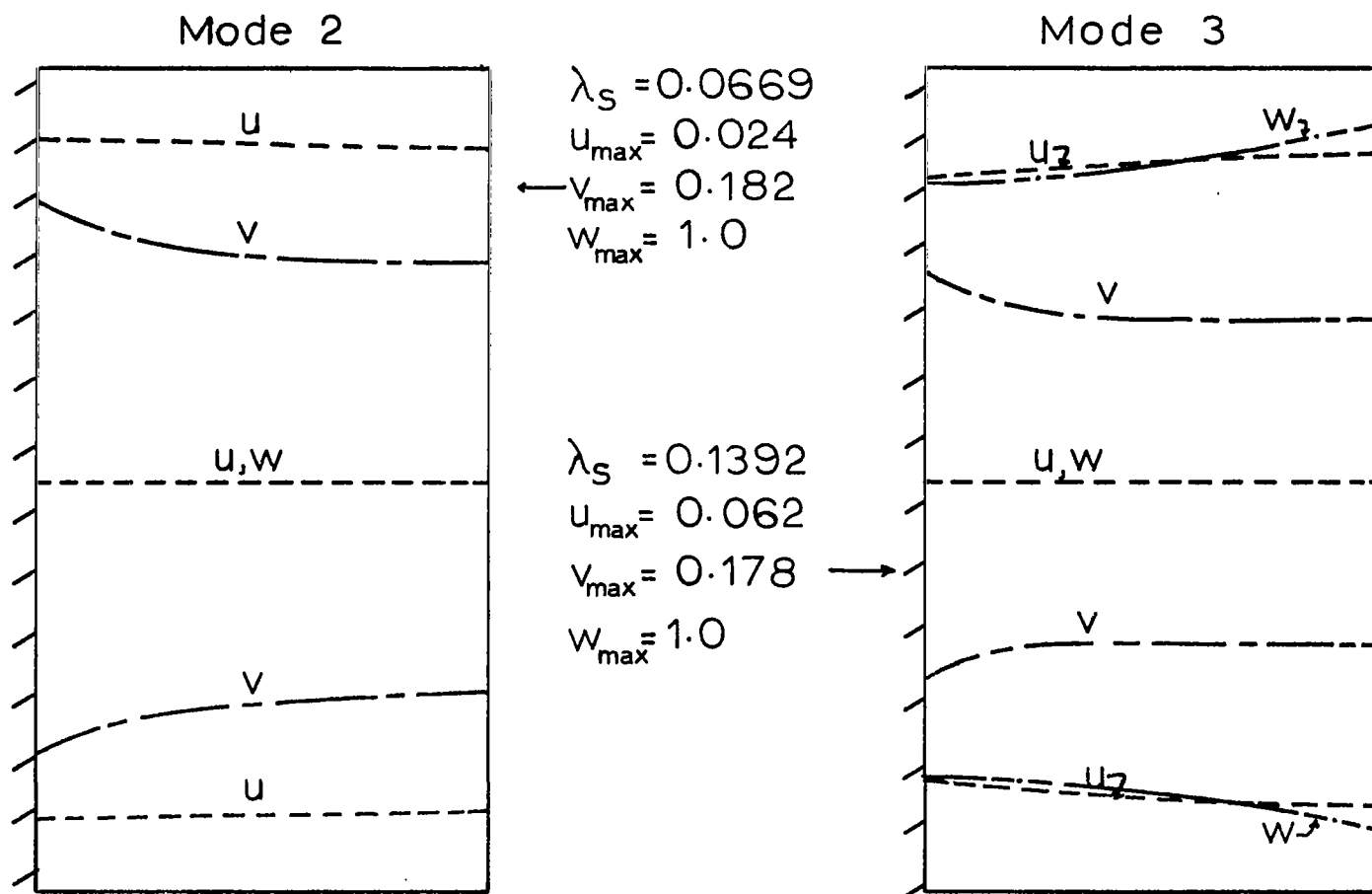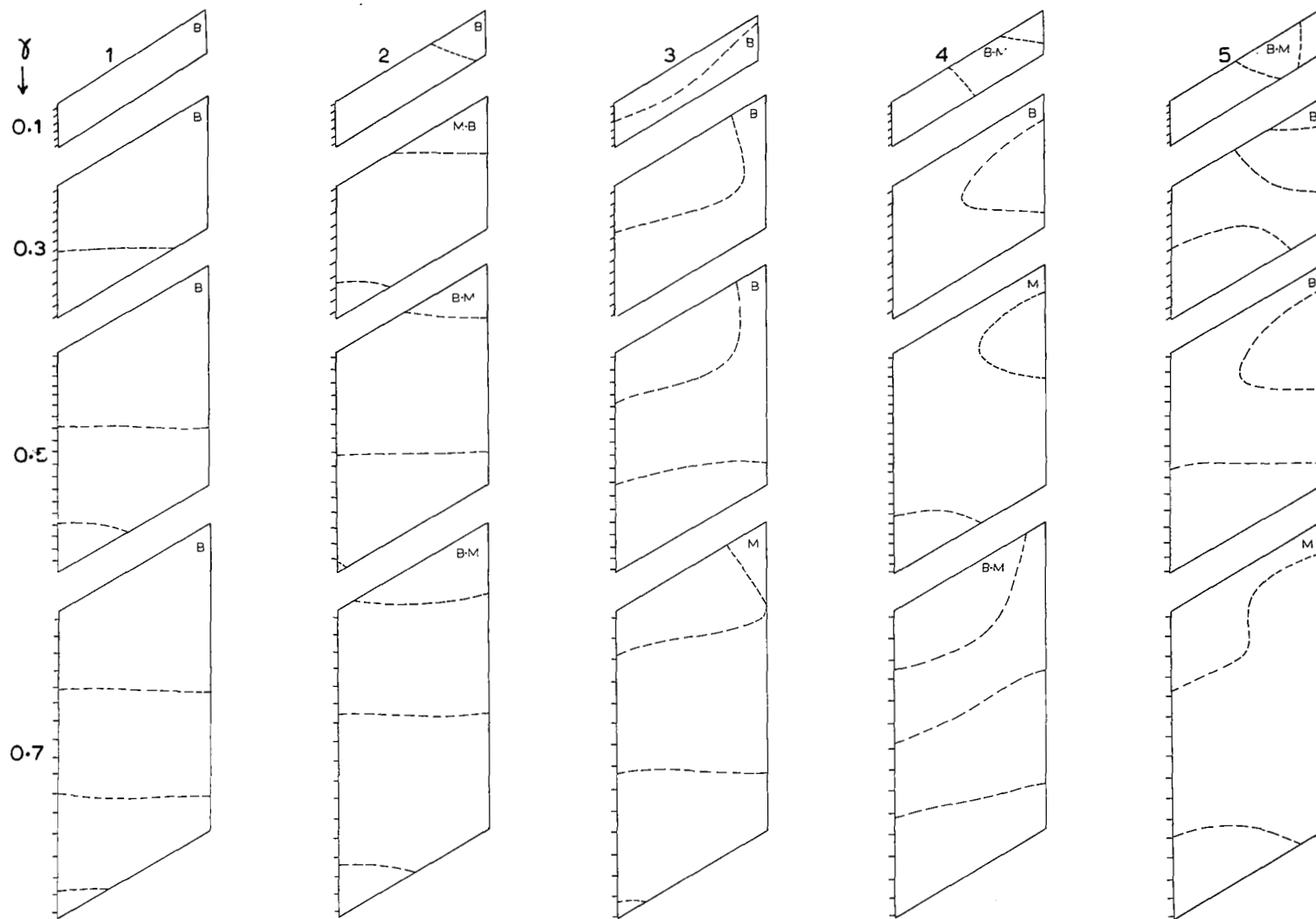Figure 20. HELICOIDAL SHELL, w NODAL PATTERNS, $\ell/R = 0.8$, $h/R = 0.01$, $\alpha = 0°$

Mode 2   Mode 3

$\lambda_S = 0.0669$
$u_{max} = 0.024$
$\leftarrow V_{max} = 0.182$
$W_{max} = 1.0$

$\lambda_S = 0.1392$
$u_{max} = 0.062$
$V_{max} = 0.178 \longrightarrow$
$W_{max} = 1.0$

FIGURE 21. DISPLACEMENT NODAL PATTERNS FOR HELICOIDAL SHELL, $l/R = 0.8$, $h/R = 0.01$, $\alpha = 0°$, $\gamma = 0.7$

Figure 22. HELICOIDAL SHELL, w NODAL PATTERNS, $\ell/R = 0.8$, $h/R = 0.01$, $\alpha = 30°$

Mode No. →

γ

80
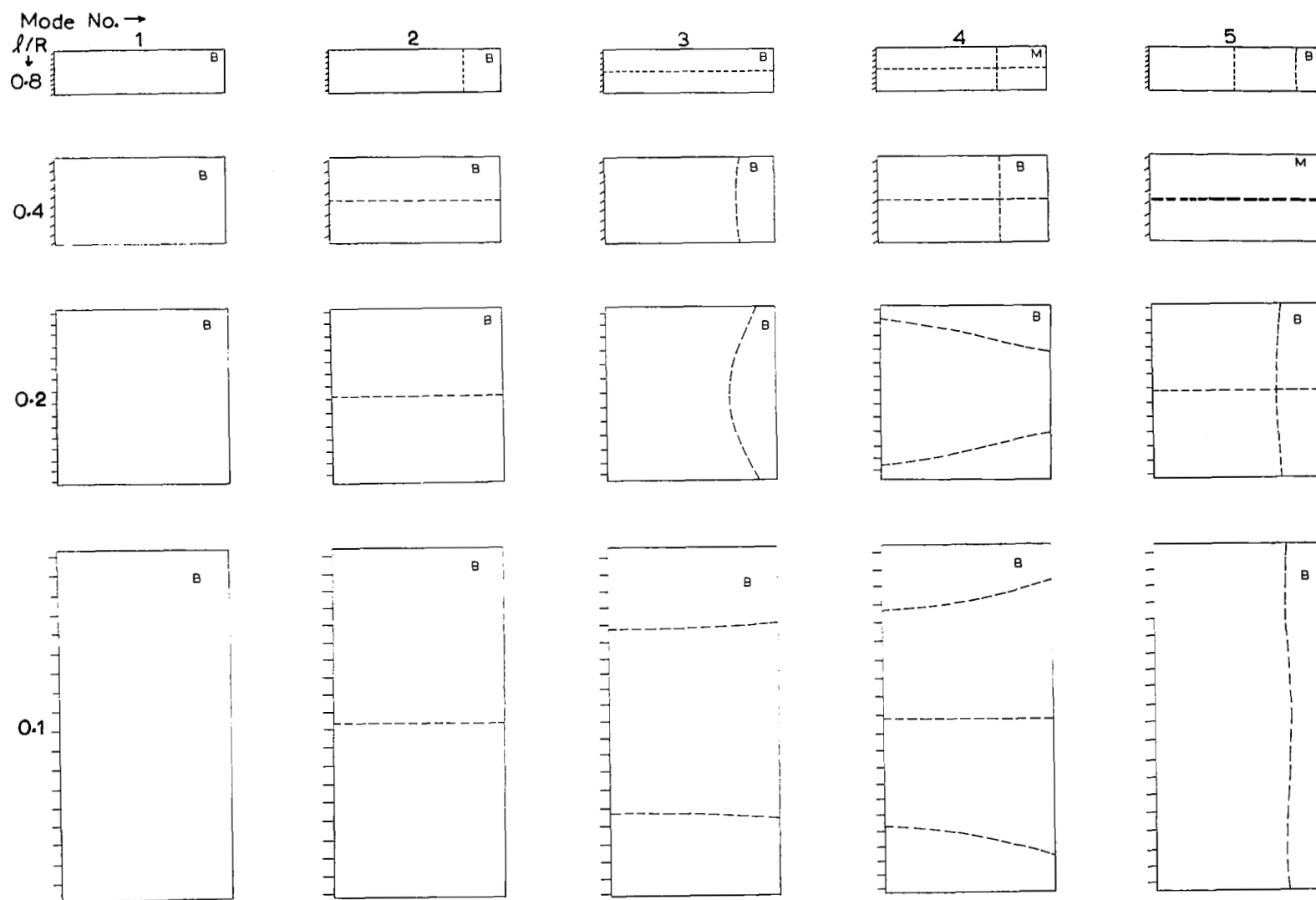
Figure 23. HELICOIDAL SHELL, w NODAL PATTERNS, h/R = 0.01, α = 0°, γ = 0.1 rad

Mode No. →

ℓ/R

1

0.8

0.4

0.2

2

3

4

5

B·M

B·M

B

B

B

M

B

B

B

B

B

B

B

B

B

B

B

B

B

B

B

70